

Cite this: *Analyst*, 2021, **146**, 5779

Engineering of nanomaterials for mass spectrometry analysis of biomolecules

 Hongmei Xu, ^{a,b} Zhenzhen Zhang,^a Yihan Wang,^a Weifeng Lu^a and Qianhao Min ^{*a}

Mass spectrometry (MS) based analysis has received intense attention in diverse biological fields. However, direct MS interrogation of target biomolecules in complex biological samples is still challenging, due to the extremely low abundance and poor ionization potency of target biological species. Innovations in nanomaterials create new auxiliary tools for deep and comprehensive MS characterization of biomolecules. More recently, growing research interest has been directed to the compositional and structural engineering of nanomaterials for enriching target biomolecules prior to MS analysis, enhancing the ionization efficiency in MS detection and designing biosensing nanoprobes in sensitive MS readout. In this review, we mainly focus on the recent advances in the engineering of nanomaterials towards their applications in sample pre-treatment, desorption/ionization matrices and ion signal amplification for MS profiling of biomolecules. This review will provide a toolbox of nanomaterials for researchers devoted to developing analytical methods and practical applications in the biological MS field.

Received 13th May 2021,
Accepted 20th July 2021

DOI: 10.1039/d1an00860a

rsc.li/analyst

1. Introduction

Mass spectrometry (MS) is a powerful tool that enables the detection of molecules by their mass to charge ratio and further declaration of the detailed structures by tandem MS (MS/MS) analysis.¹ Due to its ultra-low detection limit and wide detection range (up to 200 kDa),^{2,3} MS based analytical

methods have demonstrated their unique advantages in the fields of proteomics, lipidomics, forensics, clinical diagnostics, biomedicine, *etc.*^{4,5} Among them, soft ionization techniques such as matrix-assisted laser desorption/ionization (MALDI)⁶ and electrospray ionization (ESI)⁷ have been essential tools in the MS analysis of biological molecules.

In spite of the rapid advancement in instrumentation and analytical methods of MS technology, direct MS interrogation of target biomolecules in complex biological samples is still challenging. The low abundance of target species and severe interference from coexisting counterparts both blocked direct MS readout.^{8–10} On the other hand, there is a huge difference

^aState Key Laboratory of Analytical Chemistry for Life Science, Chemistry and Biomedicine Innovation Center, School of Chemistry and Chemical Engineering, Nanjing University, Nanjing 210023, P. R. China. E-mail: minqianhao@nju.edu.cn
^bInstitute of Environmental Science, Shanxi University, Taiyuan 030006, P. R. China



Hongmei Xu

Hongmei Xu received her PhD from Nanjing University in 2020. She is currently a professor at the Institute of Environmental Science, Shanxi University. Her current research focuses on developing innovative biomass spectrometry approaches and constructing multifunctional nanomaterials for biosensing.



Zhenzhen Zhang

Zhenzhen Zhang is pursuing a PhD in analytical chemistry at Nanjing University. Her research interests include multiplex detection and imaging of biomarkers using mass barcoded nanoprobes.

between the ionization efficiencies of diverse analytes according to their intrinsic properties, thus causing certain molecules of biological significance to be insensitive to MS analysis.^{11,12} The development of nanotechnology provided a valuable approach to solve the above problems.¹³ For example, due to their tunable composition and modifiable surface, nanomaterials can be engineered to be adsorption media for the separation and enrichment of target analytes while eliminating the interference of salts and undesired biomolecules.^{14,15} Up to now, there have been a number of nanomaterials that present a porous structure and specific affinity for pre-concentration of the desired proteins and peptides in MS-based proteomic workflows.^{16–18} On the other hand, nanomaterials are also used as matrixes to facilitate the ionization of small biomolecules in MS detection. Highly dispersed nanomaterials with excellent energy absorption and transferring capability and favorable shot-to-shot reproducibility provide a high possibility for MS analysis and quantitation of biomolecules with low molecular weights (MW < 500 Da). In addition, as for the sensing of biomolecules with low content and ionization efficiency, some signal amplification nano-probes, especially noble metal nanoparticles, show outstanding performance in translating the specific recognition events into ion signals of surface-decorated mass tags or metal clusters in an amplified, multiplexed and high-throughput detection mode.^{19–22}

In this review, nanomaterials with different compositions and functionalized surfaces used in MS analysis are summarized and classified according to their functions. In general, these functional nanomaterials are applied in three aspects in assisting sensitive MS readout: sample pre-treatment to concentrate analytes, desorption/ionization matrices to assist ionization and amplification biosensors to sensitively detect targets. In the aspect of pre-treatment of samples, we carefully survey and discuss the compositions and surface functionalization of nanomaterials and their performance for capturing endogenous peptides, phosphorylated peptides and glycosylated peptides. As for desorption/ionization matrices, various kinds of materials with different compositions (silicon-based

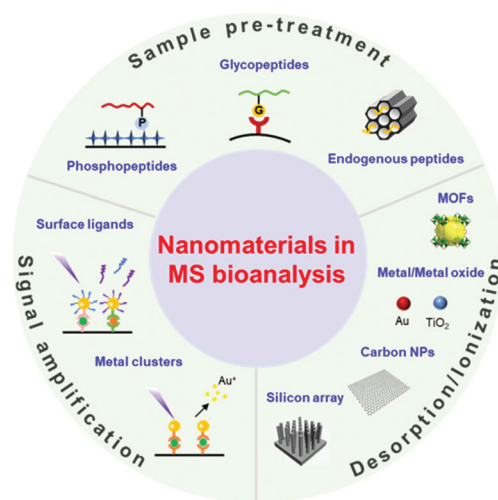


Fig. 1 An overview of nanomaterial-facilitated MS analysis of biomolecules.

nanomaterials, metal nanoparticles, metal oxides, carbon-based nanomaterials, organic frameworks, *etc.*) and their application in mass spectrometry detection and imaging (MSI) are systematically discussed. The last section provides an overview of functional metal nanoparticles used as sensing nano-probes to explore the cellular uptake process and assay various biomarkers, based on the decoded MS signal of surface ligands or metal clusters of nano-probes (Fig. 1). In the end, we also present the outlook of nanomaterials design and improvement to optimize the performance of mass spectrometry and nanotechnology in the biochemistry field.

2. Nanomaterial-mediated sample pre-treatment prior to MS analysis

2.1 Selective enrichment of low-abundance peptides

Effective identification and characterization of peptides based on MS analysis plays crucial roles in biomarker discovery and



Yihan Wang

Yihan Wang is pursuing a PhD in analytical chemistry at Nanjing University. Her research interests focus on nucleic acid and protein analysis using functional nano-probes combined with mass spectrometry.



Weifeng Lu

Weifeng Lu is currently doing his doctoral studies in analytical chemistry at Nanjing University. His research interests lie in the study of mechanisms of electrochemical organic reactions using electrochemical real-time mass spectrometry.

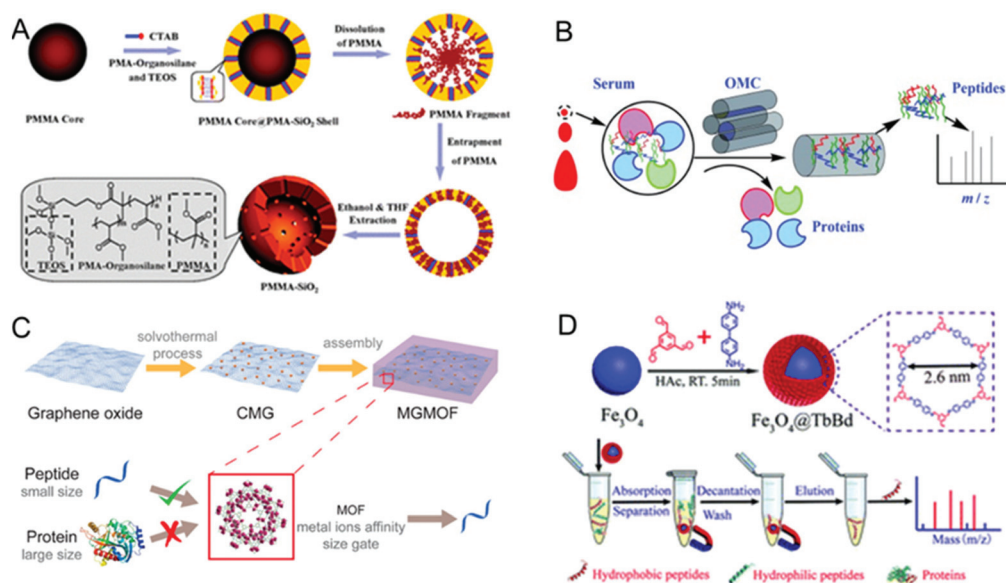


Fig. 2 Representative enrichment strategies for capturing endogenous peptides. (A) Schematic formation of PMMA-PMA-SiO₂ HMNs based on the "dissolution and entrapment" strategy. Reprinted with permission from ref. 29. Copyright (2012) Royal Society of Chemistry. (B) Enrichment of serum endogenous peptides by OMC. Reprinted with permission from ref. 14. Copyright (2011) Wiley-VCH. (C) Schematic representation of MGMOF composites and size-selection separation. Reprinted with permission from ref. 35. Copyright (2014) American Chemical Society. (D) The synthesis of magnetic COFs for the adsorption of hydrophobic peptides. Reprinted with permission from ref. 37. Copyright (2017) Royal Society of Chemistry.

disease diagnosis. In particular, some ordinary peptides relative to post-translational modification (PTM) peptides, such as endogenous peptides,²³ are of great significance in searching for disease biomarkers and exploring cancer pathogenesis.^{24,25} However, direct analysis of the above endogenous peptides is still a challenging task due to their low abundance, high dynamic range and strong interference from abundant proteins, salts, lipids and so on.²⁶ Nanomaterial mediated specific separation and concentration prior to MS identification is in high demand for detection of trace peptides from complex biological samples.

Mesoporous nanomaterials are suitable candidates for selective enrichment of endogenous peptides in real biological samples.²⁷ Generally, multiple target peptides can be effectively adsorbed in the pores of nanomaterials by combining

the size-exclusive mechanism and hydrophobic–hydrophobic interaction. Mesoporous silica, possessing large surface area, ordered mesoporous structure and easily modifiable surface, was applied for the first time in extracting endogenous peptides from human plasma by Zou and co-workers.²⁸ Most non-fitted proteins in plasma could be effectively excluded and endogenous peptides (~2721) in the mouse liver extract were detected with the integrated SCX-MCM-41 and SAX-MCM-41. Yang *et al.* utilized a dissolved polymer core to synthesize polymer–inorganic hybrid hollow mesoporous nanospheres, which exhibited a larger surface area and higher absorption efficiency (Fig. 2A).²⁹ Moreover, a series of functional mesoporous silicas such as magnetic mesoporous silica³⁰ and mesoporous silica immobilized with metal ions³¹ were proposed in sequence, both of which demonstrated their outstanding abilities in enriching the endogenous peptides. Another mesoporous nanomaterial is ordered mesoporous carbon material (OMC), which shows stronger retention of peptides compared to mesoporous silica. The Zou group developed ordered mesoporous carbon to extract the endogenous peptides from human serum.¹⁴ The distinct hydrophobicity of carbon and size exclusion ability resulted in the enrichment of a broad spectrum of endogenous peptides from serum (Fig. 2B). To further improve the poor dispersibility of carbon-based materials, different surface functionalization strategies or preparation of hybrid materials were proposed to enhance the enrichment efficiency.^{32,33}

Metal–organic frameworks (MOFs) and covalent organic frameworks (COFs) are a new category of porous crystalline materials and have attracted great interest in the research field of sample pre-treatment. In addition to their ability to capture



Qianhao Min

Qianhao Min received his PhD in analytical chemistry from Nanjing University in 2012. After working as a visiting scholar at Stanford University, he joined the faculty of Nanjing University as an associate professor in 2015. His research interests include nanomaterial-facilitated mass spectrometry, operando mass spectrometry, and nano-structured drug delivery systems.

peptides that originated from hydrophobic ligands and ordered nanopore structures, specific interaction with ligands and metal ion affinity in MOFs also enhance their enriching ability compared to mesoporous silica and carbon. To optimize their separation efficiency, magnetic nanoparticles were generally selected as the support for MOF immobilization. Zhao *et al.* fabricated a polydopamine-modified hydrophilic magnetic zeolitic imidazolate framework ($\text{Fe}_3\text{O}_4@\text{PDA}@\text{ZIF-8}$) to separate low-abundance peptides from BSA and HSA tryptic digests.³⁴ PDA is an appropriate bridge for chelating with metal ions to assemble the MOF structure, which is also contributing to the good dispersibility of nanomaterials in aqueous solution. Besides, due to the specific affinity between Zn^{2+} and histidine residues, this nanocomposite effectively eliminated the interference from histidine-poor proteins and achieved excellent enrichment of low-abundance peptides. Zheng *et al.* prepared graphene-MOF composite materials for selective extraction and separation of low-concentration peptides.³⁵ Using magnetic nanoparticles and carboxylic groups on the surface of graphene as the backbone and template for the assembly of Fe MOFs, respectively, these materials exhibited excellent separation performance towards peptides based on size selective extraction and specific affinity between metal ions and peptides (Fig. 2C). COFs are another class of organic framework nanomaterials that show their preference for hydrophobic peptides relative to MOFs.^{36,37} Lin *et al.* prepared core-shell structured magnetic covalent organic framework composites to enrich peptides from human serum.³⁷ These $\text{Fe}_3\text{O}_4@\text{TbBd}$ nanospheres exhibited high adsorption capacity and excellent reusability for peptides due to their high surface area ($196.21 \text{ m}^2 \text{ g}^{-1}$), narrow pore size distribution ($\sim 2.8 \text{ nm}$) and strong magnetic response (Fig. 2D).

Ma *et al.* systematically synthesized different sizes of spherical COFs to capture ultra-trace C-peptides from human serum and urine samples.³⁸ The high specific surface area accounted for the higher adsorption capacity, and the hydrophobicity and mesoporous microenvironment resulted in superior separation efficiency.

2.2 Selective enrichment of phosphorylated peptides

Protein phosphorylation is one of the most important post-translational modifications involved in many biological processes including cellular growth, division, and apoptosis.³⁹ To date, due to the low abundance and poor ionization efficiency of phosphopeptides, specific enrichment of phosphorylated peptides has become an imperative step in MS-based phosphoproteomics.⁴⁰ Immobilized metal ion affinity chromatography (IMAC), metal oxide affinity chromatography (MOAC) and amine-based affinity have been the main extract strategies for capturing phosphopeptides.^{41,42} This section will focus on the constituent nanomaterials of these affinity strategies and their corresponding performance in phosphopeptide enrichment.

The composition and surface modification of nanomaterials are two primary parameters that affect the enrichment performance. As for IMAC-based nanomaterials, different metal ions and surface ligands show differentiated

capture efficiency. Many efforts have been devoted to developing valuable chelating ligands to functionalize the surface of nanoparticles to satisfy the needs of efficient separation of phosphopeptides from complex samples. Iminodiacetic acid (IDA) and nitrilotriacetic acid (NTA) are two typical linkers for immobilizing metal ions, each of which can connect with one metal ion.⁴³ Subsequently, many new chelators with strong coordinating ability are also produced, such as phosphate (PO_3^{2-}),⁴⁴ adenosine triphosphate (ATP),⁴⁵ dopamine⁴⁶ and so on. Dopamine is an ideal chelating ligand to bond with various metal ions based on the catechol hydroxyl groups. The most distinct advantage is that it can be modified onto any substrates such as graphene, Fe_3O_4 nanoparticles, mesoporous silica, and target plates by its oxidative self-polymerization.^{47–49} Apart from dopamine, the phosphate ligand is another popular chelator to enrich phosphopeptides. According to metal(IV) phosphate chemistry, a metal ion could coordinate with multiple phosphate groups *via* an MO_6 octahedral coordination model, thereby affording more affinity sites for capturing phosphopeptides.⁵⁰ The Zou group developed phosphate ligand grafted $\text{Fe}_3\text{O}_4@\text{SiO}_2$ nanoparticles to immobilize titanium ions for the enrichment of phosphopeptides from digests of Arabidopsis (Fig. 3A).⁵¹ By using a PEG brush as the hydrophilic connector, this novel nanomaterial ($\text{Fe}_3\text{O}_4@\text{SiO}_2@\text{PEG-Ti}^{4+}$) presented more active sites for immobilizing titanium ions and good dispersibility in loading solution, resulting in better enrichment performance (2447 phosphopeptides) than the traditional $\text{Fe}_3\text{O}_4@\text{SiO}_2\text{-Ti}^{4+}$ (1186 phosphopeptides). Compared to a single phosphate group, ATP exhibited stronger adsorption to phosphopeptides as its three phosphate groups could chelate more metal ions. Besides, due to the intrinsic pentose sugar groups and purine base, ATP decorated nanomaterials exhibited better hydrophilicity and excluded the non-specific adsorption of nonphosphopeptides in mixtures. Zhang *et al.* have fabricated an adenosine phosphate- Ti^{4+} functionalized magnetic mesoporous graphene oxide nanocomposite ($\text{MG@mSiO}_2\text{-ATP-Ti}^{4+}$) to extract phosphopeptides from nonfat milk digest and human saliva and serum.⁴⁵

In MOAC-based nanomaterials, TiO_2 and ZrO_2 are the commonly used separation media, which are always decorated onto different substrates to construct hybrid nanoparticles. Zhang *et al.* grafted titania nanoparticles onto polydopamine-coated graphene *via* a simple hydrothermal treatment (Fig. 3B).⁵² Apart from the typical affinity that originated from Ti^{4+} , the excellent hydrophilicity introduced by the PDA interface promoted faster enrichment ability. Finally, a total number of 556 phosphorylation sites were identified from the digests of mouse brain proteins. Apart from graphene, other substrates such as magnetic nanoparticles, carbon nanotubes and silica were also exploited as the supporting substrates of metal oxides.^{53–55} Moreover, because different metal ions show unique preference for mono- or multi-phosphopeptides, nanomaterials equipped with multiple metal affinity sites may achieve comprehensive characterization of phosphopeptides. Our group prepared a ternary nanocomposite of magnetite/

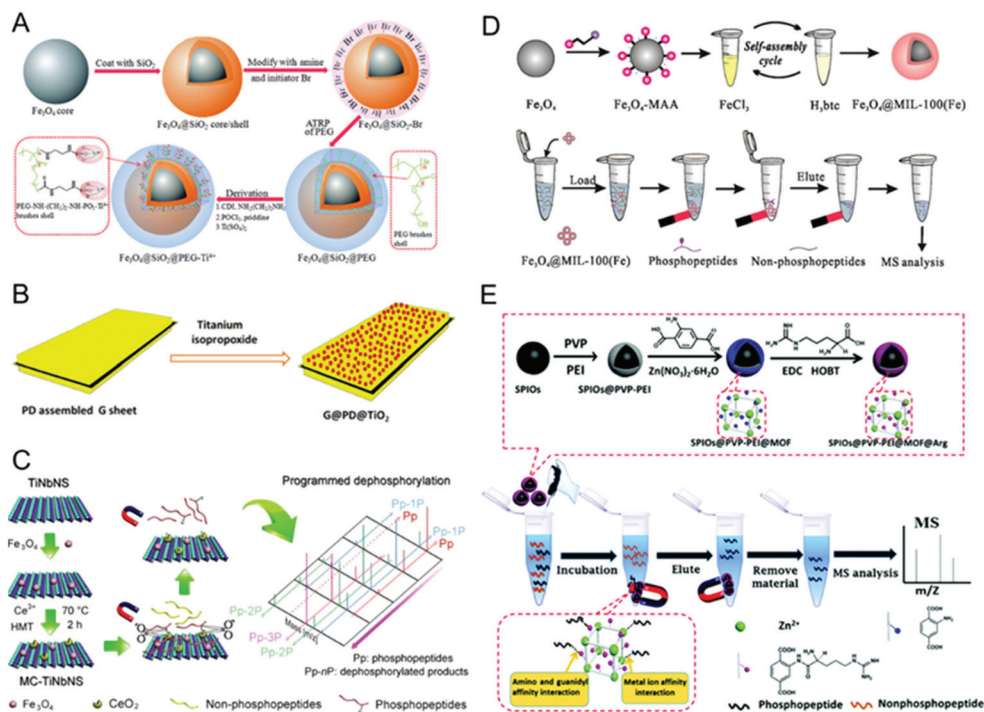


Fig. 3 Representative enrichment strategies for capturing phosphopeptides. (A) Synthesis of the PEG brush decorated magnetic Fe_3O_4 @ SiO_2 nanoparticles and immobilization of Ti^{4+} ions to form Fe_3O_4 @ SiO_2 @PEG- Ti^{4+} . Reprinted with permission from ref. 51. Copyright (2012) Royal Society of Chemistry. (B) Schematic illustration for the preparation of G@PD@TiO_2 . Reprinted with permission from ref. 52. Copyright (2014) American Chemical Society. (C) Schematic diagram of the synthetic strategy for the MC-TiNbNS composite and the mechanism of phosphopeptide enrichment and dephosphorylation. Reprinted with permission from ref. 56. Copyright (2015) American Chemical Society. (D) Preparation of Fe_3O_4 @MIL-100 for selective enrichment of phosphorylated peptides. Reprinted with permission from ref. 62. Copyright (2015) American Chemical Society. (E) Schematic representation of the synthesis and phosphopeptide enrichment of the SPMA nanospheres. Reprinted with permission from ref. 17. Copyright (2018) Royal Society of Chemistry.

ceria-codecorated titanoniobate nanosheets (MC-TiNbNSs) for the enrichment of mono- and multi-phosphopeptides and subsequent programmed dephosphorylation.⁵⁶ By altering the on-sheet CeO_2 coverage, the dephosphorylation activity could be flexibly tuned, thus achieving precise counting of the phosphorylation sites of phosphopeptides (Fig. 3C). Taking advantage of the outstanding dephosphorylation capacity of CeO_2 , we also synthesized MOF-templated porous CeO_2 to assess the activity and inhibition of multiple protein kinases based on post-enrichment dephosphorylation of phosphorylated products mediated by relevant kinases.⁵⁷ With the exception of an intentional combination of different metal oxides to construct hybrid nanomaterials, one-step synthesis of nanomaterials with multiple metal affinity sites such as NiCoMnO_4 , CuFeMnO_4 , and $\text{CaCuSi}_4\text{O}_{10}$ simplified experimental procedures and guaranteed satisfactory enrichment efficiency towards phosphopeptides, simultaneously.^{58,59}

MOFs are a class of similar MOAC-based nanomaterials due to their inherent metal-oxygen units in the structure. The adequate metal centers and microporous structure of MOFs empowered their outstanding ability in phosphopeptide enrichment. The lanthanide MOF ($[\text{Er}_2(\text{PDA})_3(\text{H}_2\text{O})]2\text{H}_2\text{O}$) was employed for the first time to capture phosphopeptides in 2013.⁶⁰ Afterwards, Zr-based MOFs such as UiO-66 and UiO-67

were successfully exploited to extract phosphopeptides from human serum.⁶¹ To further improve its separation performance, Zhang *et al.* decorated MIL-100 onto magnetic nanoparticles by layer-by-layer assembly.⁶² The synthesized nanoparticles presented a large surface area ($168.88 \text{ m}^2 \text{ g}^{-1}$), high binding capacity to β -casein tryptic digest (60 mg g^{-1}), low detection limit (0.5 fmol) and satisfactory specificity to phosphopeptides in complicated samples (Fig. 3D).

Relying on the electrostatic interaction and hydrogen bonding between amino groups and phosphate groups, amino-based nanomaterials also attracted increasing attention. The guanidino group, carrying three amine groups, has been a potential candidate moiety for specific enrichment of phosphopeptides.⁶³ However, given that guanidino-based capture is susceptible to loading solution and washing steps, a combination of multiple affinity strategies could improve the enrichment performance towards phosphopeptides.⁶⁴ Accordingly, a magnetic guanidyl-functionalized MOF with multi-affinity sites was developed by the Wu group.¹⁷ In this probe, a Zn-O cluster served as a metal affinity site to recognize phosphopeptides, while an arginine decorated organic building block further strengthened this ability based on a formative “salt bridge” between guanidyl units and phosphate groups. As a result, a total of 1659 phosphopeptides including

96.8% mono-phosphopeptides and 3.2% multi-phosphopeptides were identified from rat brain extracts (Fig. 3E).

2.3 Selective enrichment of glycosylated peptides

Glycosylation is another pivotal post-translational modification of proteins, which is involved in a series of biological processes including protein folding, cell–cell communication and cell metabolism.⁶⁵ MS-based proteomics shows outstanding potential in comprehensive profiling of glycosylated proteins.⁶⁶ However, the diversity of glycans and the low-abundance of glycoproteins make direct identification in complex samples challenging. Nowadays, nanomaterials involved in several enrichment strategies have emerged to settle the above problems, including lectin-functionalized nanobeads, hydrophilic interaction liquid chromatography (HILIC) nanomaterials and covalent interaction-based enrichment media. All of them will be discussed in this section.

Lectins are a class of carbohydrate binding proteins and are generally decorated onto the surface of different nanomaterials to selectively capture *N*- or *O*-glycopeptides and glycoproteins.^{67–70} Wang *et al.* proposed concanavalin A-chelating magnetic nanoparticles (Con A-MNPs) for selective enrichment of glycoproteins. By virtue of the Cu(II) cation mediated immobilization, the decorated content of Con A was up to 28 wt%, thus exhibiting remark-

able enrichment performance and satisfactory selectivity towards glycoproteins (Fig. 4A).⁶⁹ However, this specific affinity between one lectin and a unique glycan motif limits the identification of glycoproteins on a large scale. Ferreira *et al.* developed multiple lectin-decorated magnetic nanoprobe using suberic acid bis-*N*-hydroxysuccinimide ester as a crosslinker to strengthen the enrichment efficiency of glycoproteins from human body fluids.⁷⁰

Considering that hydrophilic glycan moieties of glycopeptides show a specific relationship with polar materials, HILIC has been widely applied in separating glycopeptides from highly abundant hydrophobic peptides.^{71,72} A number of substrate nanomaterials, such as magnetic particles,⁷³ metal-organic frameworks (MOFs),⁷⁴ and polysaccharides,⁷⁵ have been used for functionalization with hydrophilic components for glycopeptide enrichment. Liu *et al.* developed a maltose-functionalized MOF, MIL-101(Cr)-maltose, for the enrichment of *N*-linked glycopeptides *via* a two step post-synthetic modification of MIL-101(Cr)-NH₂.⁷⁴ Due to the numerous hydrophilic maltose groups, this nanomaterial showed high efficiency and sensitivity in glycopeptide enrichment from complex biological samples.

Though HILIC-based enrichment shows a wider coverage of glycopeptides, the strength of this interaction largely depends on the peptide backbone or the composition of glycan. To

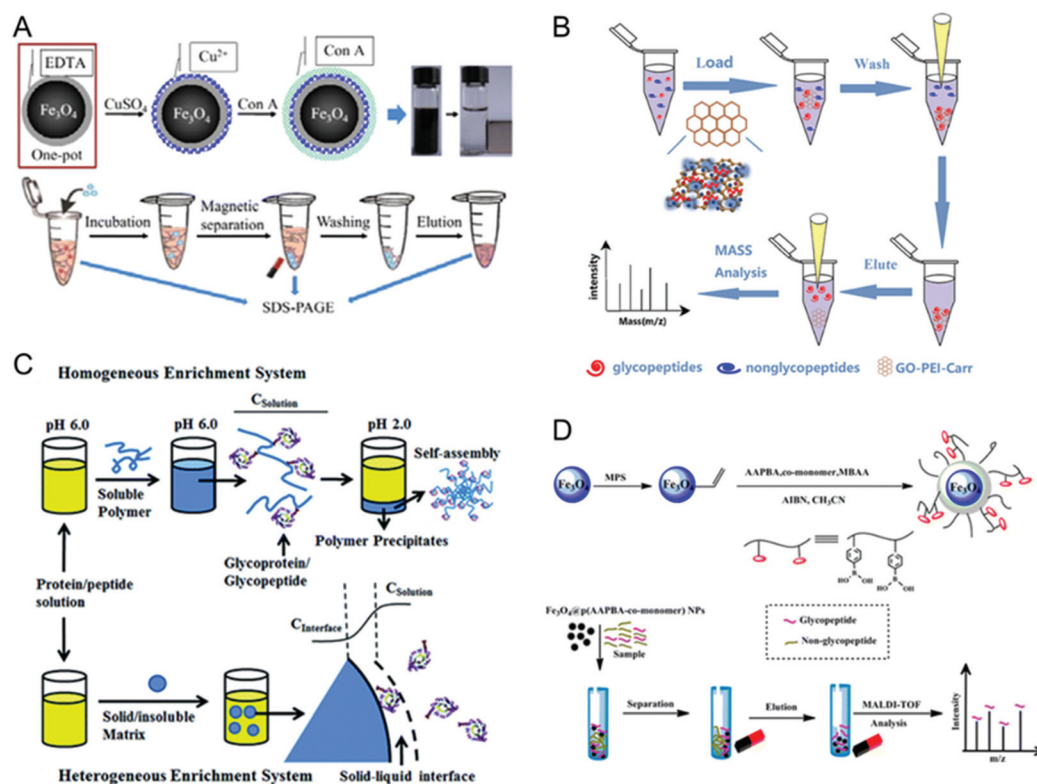


Fig. 4 Representative enrichment strategies for capturing glycopeptides. (A) Synthesis of EDTA-functionalized magnetic nanoparticles for Con A-mediated enrichment of glycopeptides. Reprinted with permission from ref. 69. Copyright (2015) American Chemical Society. (B) Demonstration of glycopeptide enrichment from protein digestion using GO-PEI-Carr. Reprinted with permission from ref. 76. Copyright (2019) American Chemical Society. (C) Schematic overview of the soluble polymer and solid/insoluble matrix based glycoprotein/glycopeptide enrichment. Reprinted with permission from ref. 77. Copyright (2015) Royal Society of Chemistry. (D) Scheme for the synthesis of Fe₃O₄@P(AAPBA-co-monomer) NPs and application in capture glycopeptides. Reprinted with permission from ref. 83. Copyright (2015) American Chemical Society.

reinforce the interaction between glycopeptides and HILIC materials, many researchers were devoted to combining HILIC with other enrichment strategies, such as integrated electrostatic interactions. Lan *et al.* decorated a graphene oxide-poly(ethylenimine) nanocomposite with carrageen, whose abundant hydrophilic groups and electronegativity enhanced the affinity to glycopeptides with a positive charge under acidic conditions.⁷⁶ Eventually, 149 glycopeptides from 129 glycoproteins with 157 *N*-glycosylation sites were identified from mouse liver tissues (Fig. 4B).

Covalent interaction-based enrichment of glycopeptides is a more universal extraction route, since chemical binding is not affected by the variation of glycan structures. There are two common covalent bonding-dominated enrichment strategies, namely, boronic acid and hydrazide chemistry. Qin *et al.* developed a pH-responsive soluble polymer coupling with hydrazide groups to capture *N*-glycoproteins/glycopeptides.⁷⁷ This tactical polymer could be dissolved in aqueous solution at mildly acidic pH, promoting sufficient adsorption of glycopeptides. Once the system pH was lowered, the self-assembly of polymers carried with glycoproteins/glycopeptides was observed, and the polymers could be rapidly separated from reaction systems. By this approach, 1317 *N*-glycopeptides from 458 *N*-glycoproteins in mouse brain samples were quickly identified (Fig. 4C).

By virtue of reversible conjugation and release of glycopeptides, boronic acid-based enrichment attracted more attention in the site-specific analysis of glycoproteomics. The types and amount of decorated boronic acid had a great effect on the enrichment capacity. As a known functional molecule, amidophenylboronic acid (APBA) has been tethered onto various nanomaterials as the affinity handles for glycopeptide enrichment.^{78,79} Lu *et al.* selected APBA decorated Fe₃O₄ nanoparticles and conventional poly(methyl methacrylate) nanobeads to enrich glycopeptides and non-glycopeptides, respectively, which promoted good selectivity in mixture samples, excellent sensitivity for detecting glycopeptides at the subfemtomole/microliter level and improved recovery of glycopeptides of up to 90%.⁸⁰ Mercaptophenylboronic acid (MPBA) is another conventional molecule applied in constructing boronic acid-based affinity nanomaterials. Due to the inherent sulfhydryl groups, MPBA molecules were easily immobilized onto AuNPs or Fe₃O₄ nanoparticles by direct formation of Au-S or Fe-S bonds.^{81,82}

Deng *et al.* synthesized MPBA functionalized magnetic nanoparticles to capture *N*-glycopeptides from biosystems by simply mixing MPBA molecules with nanoparticles.⁸¹ A total of 230 glycopeptides derived from 93 glycoproteins with 247 glycosylation sites were identified from 1 μ L of human serum. Apart from selecting appropriate boronic acid groups, increasing the amount of boronic acid coupled to nanomaterials also contributes to improving the capture ability. Up to now, a variety of polyboronic acid functionalized nanomaterials were successively proposed. Zhang *et al.* fabricated Fe₃O₄@P(AAPBA-co-monomer) nanomaterials *via* the copolymerization of 3-acrylamino phenylboronic acid (AAPBA) and

different hydrophilic monomers.⁸³ The copolymerization of AAPBA monomers provided abundant capture sites, and hydrophilic interfaces ensured good dispersibility to improve the enrichment performance (Fig. 4D).

3. Nanomaterial-assisted desorption/ionization of analytes during MS interrogation

Ionization of molecules is another important step in generating analyte ions in MS analysis. In the ionization process, matrices generally transfer the absorbed energy to the analyte to assist with desorption and ionization under laser irradiation. Organic matrices exhibit high UV absorption within the laser wavelength, however, its inherent problems such as the co-existing matrix peaks in the low mass range below *m/z* 500 and poor reproducibility between spot to spot or sample to sample caused by inhomogeneous co-crystallization of the matrix and analyte further limit the detection of small molecules. Compared to the organic matrix, nanomaterials as matrices for laser desorption/ionization (LDI)-MS analysis have unique advantages. First, nanomaterial-assisted LDI shows a background-free mass spectrum in the low molecular weight region and excellent shot-to-shot reproducibility. Besides, some nanomaterials also serve as adsorbent media to enrich analytes from complex samples, thus concentrating the local concentration of analytes and excluding the interference of salts, simultaneously. At present, multifarious nanomaterials ranging from silicon-based nanomaterials, carbon-based nanomaterials, metal nanoparticles, metal oxides and MOFs were applied as assisted matrices for MS analysis or imaging of biological molecules.^{84–87}

3.1 Silicon-based nanomaterials for LDI-MS analysis

Silicon-based nanomaterials, mainly divided into two categories, namely, stationary phase substrates and nanostructured interfaces, were widely used in assisting small molecule ionization. By virtue of simple preparation with sol-gel methods and easy surface functionalization, SiO₂ cores have been used as versatile substrates for preparing hybrid nanomaterials for LDI analysis. Qian *et al.* prepared SiO₂@Ag nanoparticles with tunable shell thickness for analysis of glucose, in which the Ag shell assisted ionization while silica cores served as hot carriers to maintain the heat during the LDI process.⁸⁸ In addition, other SiO₂-braced composites including G@SiO₂ nanocomposites and ZrO₂-SiO₂ nanorods were also utilized in the analysis of small molecules.^{89,90} Nanostructured interfaces, including porous silicon, silicon nanowires (SiNWs) and silicon microarrays, are other forms of silicon-based matrices. The desorption-ionization on silicon (DIOS) was introduced for the first time by Siuzdak's group and applied in small molecule detection.⁹¹ This nanointerface showed silent background noise in a low mass range and at high desorption/ionization efficiency.^{92,93} However, the heterogeneous mor-

phology of the silicon surface makes the interpretation of the ionization mechanism difficult. Many efforts have been made to produce a morphology-controlled silicon interface. Silicon nanowires, prepared by vapor-liquid-solid (VLS) growth or metal assisted chemical etching (MACE), have received increased attention due to the large surface capacity and satisfactory detection sensitivity.^{94,95} With the development of lithography, other controllable arrays, such as silicon pore arrays⁹⁶ and silicon microcolumn arrays,⁹⁷ and silicon nanopost arrays^{98,99} were sequentially proposed (Fig. 5A–D). Kraus *et al.* reported a versatile particle-based route to produce dense

arrays of uniform submicron pores with a high aspect ratio in silicon.⁹⁶ The uniform porous array structure showed great potential in the sensitive detection of biosamples. Vertes *et al.* developed silicon nanopost arrays (NAPAs) to enhance the ion yields and photonic properties. This NAPA chip could detect metabolic changes in single yeast cells.⁹⁹ Recently, they further utilized NAPAs as an MSI matrix for visualization of the spatial localization of polyhydroxybutyric acid, polyglutamic acid, and polysaccharide oligomers in plant tissues.¹⁰⁰ Compared to MALDI-MSI, this NAPA-LDI-MSI showed higher ionization efficiency and wider repeat unit range coverage for oligomers of targets (Fig. 5E). Voelcker *et al.* also prepared a thin porous silicon (pSi) film to reveal the distribution of small molecular metabolites on marine mollusc tissues or fingerprints by the contact printing approach.^{101,102} The high UV cross-section and the large surface area of silicon arrays contributed to the sensitive readout and simple sampling without pre-purification, and thus they have become the majority of the nano-substrates employed in SALDI-MSI, however, harsh preparation processes limit their extensive application.

3.2 Carbon-based nanomaterials for LDI-MS analysis

With the merits of large surface areas, high optical absorption and excellent electronic properties, carbon-based nanomaterials manifested unique advantages in MS imaging and analysis of small molecules. Ranging from graphite carbon, nanotubes, fullerenes, nanodiamonds, nanofibers, nanodots and graphene,^{103–107} different types of carbon-based nanomaterials have been applied in the detection of small molecules. Guo *et al.* used carbon nanotubes (CNTs) as an LDI matrix for the first time for the analysis of small molecules.¹⁰⁸ However, the hydrophobicity of CNTs made them difficult to deposit onto a steel plate and then be co-crystallized with analytes, resulting in poor reproducibility for LDI-MS analysis. Afterwards, a variety of derivative CNTs with amendatory dispersibility were developed and further applied in small molecule analysis. Guo *et al.* developed oxidized CNTs as the LDI-MS matrix, which showed better dispersion and reproducible results due to the sufficient hydroxyl and carboxyl groups on the CNT surface.¹⁰⁹ In addition, other functional CNTs such as organic ligand-decorated CNTs or CNT-based composite materials including magnetic/oxidized CNT composites ($\text{Fe}_3\text{O}_4@\text{SiO}_2/\text{OCNT}$) and polyelectrolyte/oxidized CNTs were constructed to achieve better sensitivity and reproducibility.^{110–113}

Recently, owing to its large surface area, high thermal conductivity and energy transfer capability, graphene has also emerged as an LDI MS matrix for small molecule analysis. The Jiang group fabricated a series of functionalized graphene to assist the ionization of analytes.^{114–116} They developed antibody-functionalized graphene oxide nanoribbons as the LDI matrix, in which abundant oxygen groups improved the water dispersibility and guaranteed reproducible results, while the decorated antibody further enhanced the selectivity to a specific analyte and avoided interference from absorbed non-target compounds.¹¹⁴ Apart from oxidative modification, they

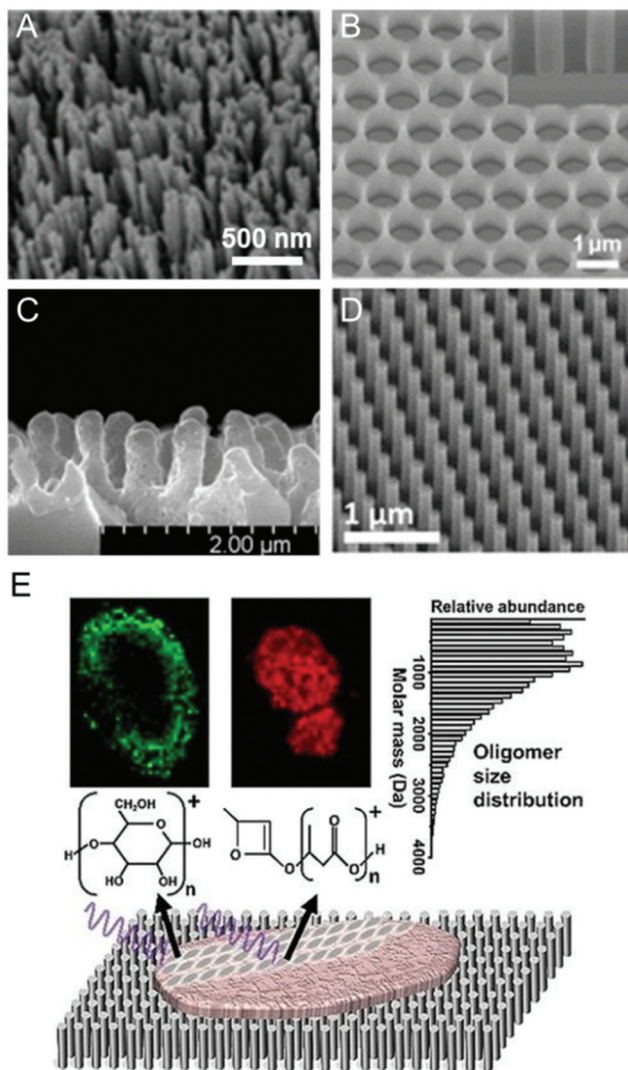


Fig. 5 Silicon-based nanomaterials for LDI-MS analysis. (A) SEM image of SiNWs. Reprinted with permission from ref. 95. Copyright (2018) American Chemical Society. (B) SEM image of silicon pore arrays. Reprinted with permission from ref. 96. Copyright (2015) American Chemical Society. (C) SEM image of silicon microcolumn arrays. Reprinted with permission from ref. 97. Copyright (2009) Wiley-VCH. (D) SEM image of silicon nanopost arrays. Reprinted with permission from ref. 99. Copyright (2016) American Chemical Society. (E) NAPA-LDI-MSI of soybean root nodule sections. Reprinted with permission from ref. 100. Copyright (2021) Wiley-VCH.

also synthesized fluorographene as the matrix for screening chemical contaminants in complex samples.¹¹⁵ Fluorination can convert the C–C bonds from the sp^2 to sp^3 configuration, thus promoting the ionization process by the formation of hydrogen bonding with analytes. Besides, fluorographene demonstrated better thermodynamical stability than other graphene derivatives, which could ensure fewer fragments and a noise-free mass spectrum in the LDI process (Fig. 6A).

However, the shedding of coated nanomaterials from a stainless steel plate under laser irradiation is inevitable. To improve the stability of the nanomaterial-based matrix, they prepared a 3D printed graphene-doped MALDI monolithic plate to replace the traditional stainless steel plate.¹¹⁶ Upon adjusting the doping amount of graphene, it could detect various environmental pollutants in both negative and positive ion modes. Heteroatom doping into graphene can considerably modulate the electronic properties to facilitate the ionization process. Our group synthesized gas-phase N-doped graphene (gNG) as the matrix for LDI-MS.¹⁰⁶ The nitrogen-provided sp^2 -hybridized frameworks contributed to efficient laser absorption and energy transfer. Besides, the electronic structure of doped nitrogen atoms also facilitated the deprotona-

tion of targets in negative ion mode. To achieve dual-ion-mode LDI MS analysis, Wang *et al.* developed an O–P, N-doped carbon/graphene matrix using phytic acid, polyaniline and graphene aerogels as the pyrolysis sources.¹¹⁷ Multiple heteroatom doping provided more defective sites and negatively charged $P-O_x^-$ groups could adsorb metal cations, which promoted the formation of sodium and potassium adducts in positive ion mode (Fig. 6B).

Carbon nanodots (CDs), as newly emerged members of carbon-based nanomaterials, have received increasing attention in LDI analysis of small molecules. Nie *et al.* proposed for the first time carbon nanodots as the matrix for analysis of small molecules in both positive and negative ion modes.¹¹⁸ Apart from the distinct elimination of the background interference in the low-mass range and uniform dispersion properties, the small size (~ 3 nm) of CDs also facilitated easier desorption of analytes and achieved more sensitive detection (Fig. 6C). In addition, they also proposed a label-free mass spectrometry imaging approach to profile the sub-organ distribution of carbon nanotubes, graphene oxide and carbon nanodots in mice by monitoring the intrinsic carbon cluster signal of the nanomaterials.¹¹⁹ The results demonstrated that most

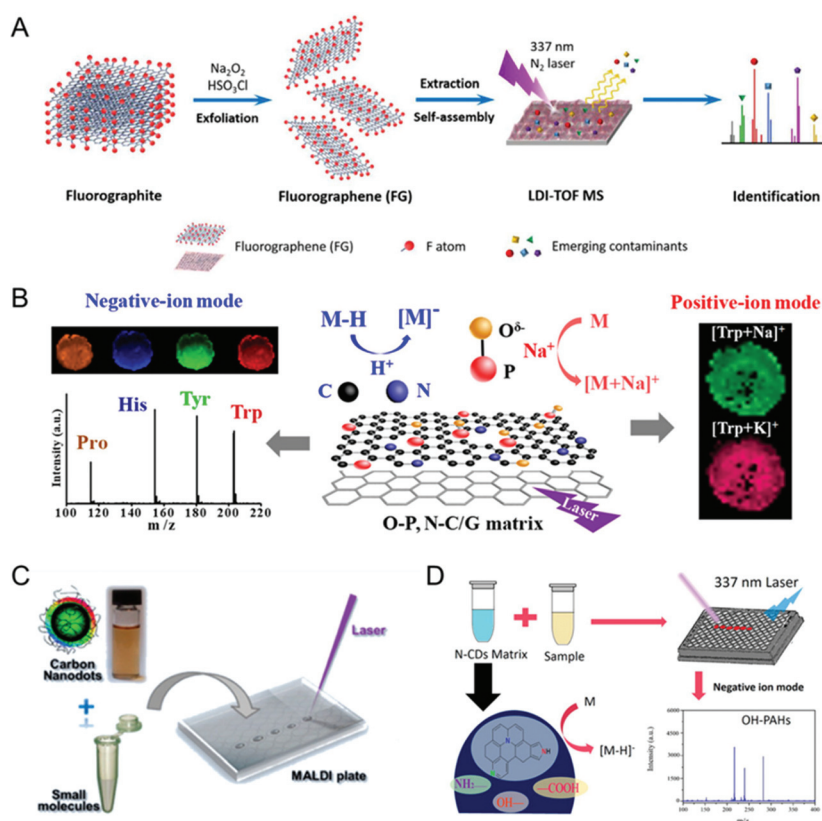


Fig. 6 Carbon-based nanomaterials for LDI-MS analysis. (A) Schematic diagrams of the procedures for screening of ECCs in complex samples by SELDI-TOF MS with FG as a probe. Reprinted with permission from ref. 115. Copyright (2017) American Chemical Society. (B) Dual-ion-mode analysis of various small compounds in MALDI-TOF MS through using a synthesized O–P, N doped carbon/graphene matrix. Reprinted with permission from ref. 117. Copyright (2018) American Chemical Society. (C) Carbon nanodots as the matrix for the analysis of small molecules. Reprinted with permission from ref. 118. Copyright (2013) American Chemical Society. (D) Synthesis of N-doped carbon dots as a matrix for the analysis of OH-PAHs. Reprinted with permission from ref. 120. Copyright (2016) American Chemical Society.

carbon nanotubes and nanodots were located in the outer parenchyma of the kidneys, and all three materials were found in the red pulp of the spleen. Cai *et al.* prepared N-doped carbon dots for negative-ion detection of hydroxy-polycyclic aromatic hydrocarbons by using DL-malic acid and ethanolamine as precursors.¹²⁰ The π -conjugated polyaromatic structure and the electronic structure of the doped nitrogen atoms both endowed the LDI analysis with high sensitivity (Fig. 6D). They also synthesized N, S-co-doped carbon dots as the matrix for MS imaging of the distribution of bisphenol S (BPS) in different mouse tissues in negative ion mode.¹²¹

3.3 Metal and metal oxide nanostructures for LDI-MS analysis

Due to the excellent optical properties and surface plasmonic resonance effect, metal-based nanomaterials, including noble metal nanoparticles and metal oxides, show high UV absorption ability and hot carrier property to enhance the desorption and ionization of analytes. Noble metal nanoparticles, mainly Au, Ag and Pt, have been frequently used for imaging and analysis of small molecules, peptides and large proteins.^{122–126} Russell *et al.* for the first time utilized AuNPs as the LDI matrix for the detection of peptides, in which both Au clusters and peptides were ionized under irradiation.¹²² Though Au clusters hindered the peak intensity of small molecules, the use of AuNPs as matrixes could reflect other information such as the thiol terminated DNA coverage or provide the possibility of internal calibration.¹²³ In addition, Au nanoparticles also showed unique advantages in the detection of glutathione or other thiol molecules due to their strong affinity to thiol compounds.¹³ However, the stronger interaction between proteins and Au nanoparticles made the desorption of the proteins difficult under certain laser energy. Pt nanoparticles were proven to be suitable for analysis of large proteins owing to their higher thermal conductivity compared to other metal nanoparticles, thus allowing the ionization of molecules with lower laser energy.^{13,124} Silver nanoparticles with tunable surface properties and excellent optical properties also showed good performance as an LDI matrix. Chen *et al.* compared the individual LDI capacities of three silver nanocrystals (cubes, cuboctahedra and octahedra).¹²⁵ Ag cuboctahedra showed the highest ionization efficiency due to the extensive appearance of hot spots caused by the homogenous dissipation of laser energy on well-oriented silver cuboctahedra. Various shapes of metal nanoparticles showed different optical and electronic properties, thus affecting the ionization efficiency. For Au nanoparticles, AuNPs, Au nanorods (AuNRs) and Au nanoshells (AuNSs), AuNSs displayed the best ionization efficiency due to their excellent energy absorption ability to generate hot carriers.¹²⁶ Apart from shapes, the size of metal nanomaterials also resulted in differentiated detection performance. Shen *et al.* have compared the LDI properties of AgNPs of three different sizes (2.8 ± 1.0 , 12.8 ± 3.2 and 44.2 ± 5.0 nm) in the analysis of amyloid-beta (A β) peptides, from which the smallest AgNPs adsorbed more analytes and produced the highest peak intensity.¹²⁷ In addition to the individual metal nano-

particles, metal-based alloy materials that exhibit tunable plasmonic properties and hot carriers also show great advantages in LDI-MS analysis of biomolecules.

Apart from serving as matrices for the analysis of biomolecules, Au and Ag nanoparticles were widely applied in imaging the distributions of cholesterol and other lipids in various organs due to the compatible applicability in either positive or negative ionization modes, in contrast to the usual MALDI matrices such as DHB or 9-AA, respectively, used in positive or negative ionization modes, thus allowing the comprehensive analysis of different small molecules. Siuzdak *et al.* developed fluorocarbon functionalized AuNPs as an LDI matrix for mass spectrometric imaging analysis of metabolites in biological tissues.^{128,129} Laser-induced release of the fluorocarbon chains provided a driving force for analyte desorption and promoted the generation of intact molecular ions (Fig. 7A). Furthermore, perfluorohexane decorated AuNPs created a hydrophobic environment on tissues to minimize metabolite solubilization and spatial dislocation, hence providing an actual picture of tissue metabolism. Taking advantage of the ability of silver to form weak charge transfer complexes with double bonds, Ag-based nanoparticles were widely used for selective imaging of long-chain unsaturated hydrocarbons. Zhao *et al.* fabricated polyvinylpyrrolidone (PVP) capped AgNPs to simultaneously analyze 10 classes of lipids from the brain by assessing the corresponding silver adducts.¹³⁰ Specifically, owing to the abundant silver ions, some compounds with poor ionization efficiency such as FAs and sterols could obviously be detected. Moreover, the metal nanoparticles used in MSI were also ionized and they produced intense signals, which could be used as the internal calibration to improve the imaging accuracy. Voelcker *et al.* proposed the use of ultrathin Ag layers as an interlayer between the pSi substrate and fingerprints to ensure mass accuracy in small-molecule measurements. According to the Ag internal calibration, the mass accuracy was improved by more than one order of magnitude in several cases (Fig. 7B).¹³¹

However, single metal nanoparticles are easy to agglomerate while excessive surfactants suppress the peak intensities of analytes. Metal-based hybrid materials provide synergistic effects to assist the ionization of analytes. A silver-gold nanoalloy was fabricated as the matrix for mass spectrometric imaging of latent fingerprints.¹³² The presence of Au suppressed the aggregation of nanoparticles while the Ag component enhanced the optical absorption efficiency, resulting in higher image sensitivity. The Qian group reported a core-shell polymer@Ag structural matrix for the identification of metabolic fingerprints from urine without enrichment or purification.¹³³ A polymer core with lighter weight and abundant surface active sites is more advantageous in preparing hybrid compounds compared to SiO₂ cores.⁸⁸ With the advantages of high UV absorption and efficient energy transfer with hot carriers, they successfully diagnosed and differentiated the subtypes of kidney diseases in clinics (Fig. 7C). Besides, other nanostructured composites such as a gold@graphitized mesoporous silica nanocomposite (Au@GMSN), gold nanoparticle

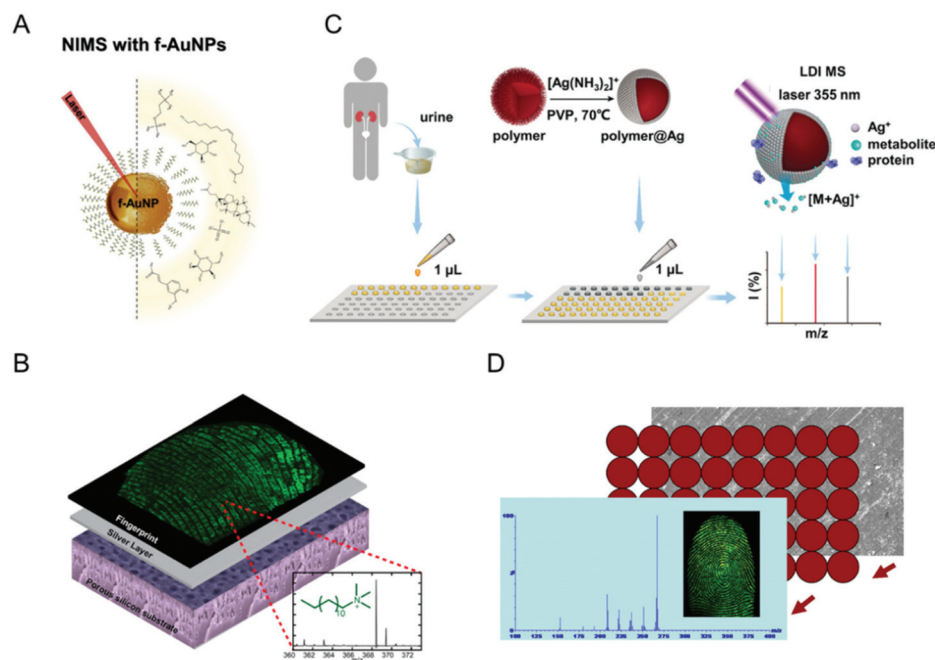


Fig. 7 Metal-based nanomaterials for LDI-MS analysis. (A) Schematic of the desorption of the perfluorinated monolayer on the surface of the f-AuNP. Reprinted with permission from ref. 129. Copyright (2018) American Chemical Society. (B) Silver coating on nanostructured silicon for high-mass-accuracy imaging of fingerprints. Reprinted with permission from ref. 131. Copyright (2015) American Chemical Society. (C) Overall schematics for the extraction of urine metabolic fingerprints (UMFs) by polymer@Ag. Reprinted with permission from ref. 133. Copyright (2020) Wiley-VCH. (D) Chemical imaging of latent fingerprints based on laser activated electron tunneling on the surface of $(\text{Bi}_2\text{O}_3)_{0.07}(\text{CoO})_{0.03}(\text{ZnO})_{0.9}$. Reprinted with permission from ref. 149. Copyright (2015) American Chemical Society.

grafted nanostructured silicon (AuNPs@nSi) surface and gold nanoshell coated microarray chip also demonstrated synergistic effects in the analysis of biomolecules.^{134,135} Apart from acting as functional shells to construct a hybrid-structure, metal nanoparticles were also fixed in confined interlayers to separate layered two-dimensional nanomaterials. Xu *et al.* developed an MoS_2/Ag hybrid for negative ion LDI analysis of small molecules.¹³⁶ AgNPs provided high UV absorption and efficient energy transfer to assist ionization, while MoS_2 nanosheets exhibited high surface roughness and a large surface area for analyte absorption, hence exhibiting good signal reproducibility and low background interferences compared to organic matrices. Lu *et al.* also reported similar structured-composites for the quantitative analysis of glucose and psoralen.¹³⁷

Metal oxides, with strong UV absorption, semiconductor properties and high melting and boiling points, have been employed as LDI matrices. Fe_3O_4 , ZnO and TiO_2 were three common matrixes for assisting analyte ionization. In spite of their advantages of quick magnetic separation and simple synthesis procedures, bare Fe_3O_4 nanoparticles showed low facilitating ionization efficiency due to their small bandgap (2.2 eV) and the lack of ability to produce cation adducts, which could be improved by surface functionalization with citric acid and glutathione (GSH).^{138,139} In addition, other magnetic nanocomposites including $\text{Fe}_3\text{O}_4/\text{PDA}$ and $\text{Fe}_3\text{O}_4/\text{Au}$ also exhibited better LDI efficiency compared with Fe_3O_4

nanoparticles.^{140,141} In particular, apart from acting as the LDI matrix and enrichment media for capture and analysis of biomolecules, TiO_2 nanoparticles also played unique roles in assisting MALDI-MS reaction monitoring due to photoreactivity. Chen *et al.* employed core-shell structured $\text{Fe}_3\text{O}_4/\text{TiO}_2$ nanoparticles to concentrate and directly detect phosphopeptides.¹⁴² The shape and size of TiO_2 nanocrystals were crucial factors to determine the desorption and ionization efficiency. It was demonstrated that TiO_2 prolate nanospheroids (TiO_2 PNSs) showed the highest sensitivity and reproducibility compared to TiO_2 nanoparticles (TiO_2 NPs) and TiO_2 nanotubes (TiO_2 NTs).¹⁴³ However, due to the low UV absorption of TiO_2 nanoparticles and their ester hydrolysis catalytic activity, TiO_2 -based phospholipid detection still faces a great challenge. Sweedler *et al.* synthesized a dopamine-modified TiO_2 monolith to address this problem. Integration with dopamine largely increased the UV absorption of TiO_2 , while an increased pH value on the TiO_2 monolithic surface also decreased the catalytic hydrolysis of the lipids, thus achieving a 10- to 30-fold increase in the signal-to-noise ratio for analyte detection.¹⁴⁴ On the other hand, taking advantage of the photocatalytic properties of TiO_2 , Girault *et al.* designed for the first time a porous TiO_2 photoelectrode on a MALDI steel plate to drive in source photoelectrochemical redox reactions. Under UV laser irradiation, the electron-hole pairs generated on TiO_2 nanoparticles were sufficient to make them photosensitizers to actuate the electron transfer with analytes. Using

Critical Review

CHCA as the matrix, they explored the tagging reaction of a cysteine-containing peptide.¹⁴⁵ Furthermore, they took advantage of the photocatalytic properties of TiO₂ to destroy bacterial cell membranes to detect the cellular components. The electron-transfer and radical reactions appeared on the TiO₂ surface, thus generating reactive oxygen species such as hydroxyl radicals and peroxide to accelerate the disruption of the bacterial envelope.¹⁴⁶ Another widely used metal oxide, ZnO, exhibited higher UV absorption compared to TiO₂ due to its large bandgap (3.2 eV). Zhong *et al.* proposed a new ionization methodology called laser activated electron tunneling (LAET).^{147–149} Upon UV laser radiation, the photoelectrons generated on the surface of ZnO could be captured by adsorbed organic molecules, which promoted the desorption and ionization of these molecules in negative ion mode (Fig. 7D).¹⁴⁹ Besides, based on the interpretation of the mass and charge information of adsorbed molecules, the photocatalytic mechanism of the materials was also figured out.

3.4 Organic frameworks for LDI-MS analysis

Metal–organic frameworks (MOFs), regarded as a new class of nanomaterials, have received intense interest due to their superior properties including high specific surface area, uniform porosity, flexible design and easy functionalization.¹⁵⁰ Although applied in diverse fields, the use of MOFs as LDI matrixes for small molecule analysis is still in its early stage. The Huang group tested for the first time the LDI properties of several MOFs including MIL-100 (Fe), MIL-100 (Cr), MIL-100 (Al), MIL-101 (Cr), DUT-4 (Al), DUT-5 (Al) and CYCU-3 (Al) and found that the types of metal ions had a great influence on the background signals and reproducibility of the results.¹⁵¹ Cai *et al.* synthesized three zeolite imidazole frameworks (ZIF-7, ZIF-8 and ZIF-90) to enrich and detect bisphenols and environmental pollutants.¹⁵² As a result, ZIF-8 showed the highest signal intensity and low background interference due to the largest surface area, which was helpful for laser energy absorption and transfer. Gu *et al.* reported for the first time bulk MOFs of 2-D Zn₂(bim)₄ nanosheets as matrixes for LDI-MS analysis of amino acids, nucleobases, neurotransmitters, hormones and pollutant molecules.¹⁵³ This matrix showed satisfactory advantages such as clean background, high salt tolerance and good reproducibility. Compared to the purposeless screening of nanomaterials, directly synthesized nanomaterials may show higher efficiency in assisting the ionization of analytes. Zou *et al.* fabricated tailor-made Zr(IV)-based metal–organic frameworks UiO-66-PDC and UiO-66-(OH)₂ using 2,5-pyridinedicarboxylic acid (PDC) and 2,5-dihydroxyterephthalic acid (DHT) as ligands, whose structures are similar to organic matrixes 2-picolinic acid (PA) and 2,5-dihydroxybenzoic acid (DHB), hence ensuring excellent UV absorption capacity.¹⁵⁴ UiO-66-(OH)₂ demonstrated great potential in the quantitative analysis of glucose and pyridoxal 5'-phosphate (Fig. 8A). Recently, nanoporous carbons derived from MOFs were also applied as novel matrixes for LDI analysis. After heating MOFs under a nitrogen atmosphere, the carbonized MOFs exhibited a higher surface area and larger pore volume

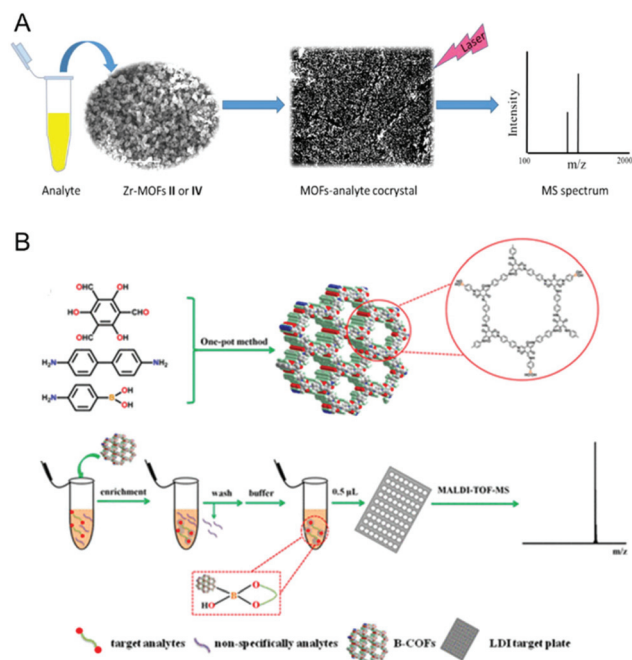


Fig. 8 Organic framework based LDI-MS analysis. (A) Design and synthesis of Zr-MOFs for LDI-MS analysis of small molecules and enrichment of phosphopeptides. Reprinted with permission from ref. 154. Copyright (2016) American Chemical Society. (B) Synthetic route for B-COFs and the selective enrichment of *cis*-diol-containing compounds. Reprinted with permission from ref. 158. Copyright (2019) American Chemical Society.

compared with carbon-based materials, and have been applied in detecting polar and nonpolar small molecules.¹⁵⁵

Covalent organic frameworks (COFs), as another category of emerging materials, exhibited high thermal stability, high surface area and adjustable pore size. Xia *et al.* reported a spherical COF TpBD as the LDI matrix for analysis of small molecules and environmental pollutants. Compared with the DHB matrix, it showed enhanced signal intensity, free matrix background and good salt tolerance.¹⁵⁶ Cai *et al.* fabricated a magnetic covalent organic framework nanomaterial (Fe₃O₄@COFs) for the concentration and detection of PAHs and derivatives in PM 2.5.¹⁵⁷ It turned out that Fe₃O₄@COFs had a clean background and higher sensitivity due to good electrical conductivity and high surface area. In addition, boronic acid-functionalized COFs were successfully synthesized and used as catchers and LDI matrixes for the selective enrichment and analysis of *cis*-diol containing molecules in both positive and negative ion modes (Fig. 8B).¹⁵⁸

3.5 Other nanomaterials for LDI-MS analysis

Apart from the use of the above nanomaterials as LDI matrixes, several 2D nanomaterials such as graphitic carbon nitride (g-C₃N₄), molybdenum disulfide (MoS₂) and h-BN were also outstanding candidates for assisting biological molecule analysis. Cai *et al.* prepared for the first time ultrathin graphitic carbon nitride (g-C₃N₄) nanosheets to serve as novel

matrixes for the detection of small molecules in negative ion mode.¹⁵⁹ These nanosheets showed free matrix background interference, good salt tolerance, increased signal intensity and 1 pmol detection limit for 1-nitropyrene (1-NP) in sewage (Fig. 9A). Nie *et al.* reported hexagonal boron nitride (h-BN) nanosheets for enrichment and imaging analysis of metabolites.¹⁶⁰ The structure of the B–H six-membered ring was a proton transporter that could assist the ionization of analytes to improve the signal-to-noise ratio and detection limit. More recently, they constructed doxorubicin (DOX)/polyethylene glycol-MoS₂ nanosheets to *in situ* monitor drug release by detecting the MS signal intensity ratio of the loaded drug to the nanocarriers. This system successfully revealed the different distribution of nanocarriers in lung, spleen, and liver tissues, and the tissue-dependent release behavior of DOX during circulation (Fig. 9B).¹⁶¹ Taking advantage of Li intercalation/exfoliation, Xu *et al.* fabricated MoS₂ nanoflakes for MS analysis of small molecules. However, the challenging preparation procedures restricted their widespread application. Rotello *et al.* used Na-assisted liquid phase exfoliation to prepare MoS₂ nanoflakes, which showed high environmental tolerance and enhanced ionization efficiency.¹⁶² Ouyang *et al.* utilized AuNPs to stabilize diphenylalanine (FF) nanosheets by using a facile electrospray method followed by a thermal treatment process, which were further applied as solid-phase

microextraction (SPME) fibers for adsorption and *in vivo* analysis of target molecules.¹⁶³

4. Amplification nanosensors for facilitating sensitive MS readout

Apart from serving as the absorbent and matrix to assist the MS analysis of target molecules, some metal nanoparticles functionalized with affinity linkers and surface ligands can be appointed as functional nanoprobess for high-sensitivity detection of target biomolecules. Based on specific recognition, detection of biomolecules of low abundance or low ionization efficiency can be transformed into assessing the abundant ion signals of surface ligands or metal clusters of functional nanoprobess. There are two types of detection strategies according to the source of ion signals.

4.1 Surface ligands on nanoprobess as the signal output

Due to the ease of surface modification, high UV absorption and good biocompatibility, AuNPs demonstrated enormous advantages in constructing functional nanoprobess. The Au–S bond was easily broken under laser irradiation, thus providing massive fragments for MS detection. Furthermore, surface ligands not only endowed the nanoprobess with outstanding signal amplification ability, but also contributed to an accurate evaluation of the biodistribution of nanoprobess.

There are several types of surface ligands, including short polyethylene glycol compounds, short-chain DNA molecules, peptides and lipids, generally termed mass tags or mass barcodes.

Rotello *et al.* proposed for the first time that AuNPs functionalized with cationic or neutral surface ligands could be used to explore the cellular uptake process.¹⁶⁴ By collecting the endocytic AuNPs and then analyzing the ion signals of surface ligands, they demonstrated that nanoparticles with different surface charges showed differential cellular uptake behavior. Furthermore, they also explored the intracellular stability of AuNPs by quantifying the monolayer detachment using parallel measurements by LDI and inductively coupled plasma (ICP) mass spectrometry (Fig. 10A).¹⁶⁵ They found that intracellular biothiols could degrade the AuNP monolayers and differently structured monolayers showed varying anti-interference ability, thereby providing new insight for the design of stable nanoparticles. Based on the above foundational research, they further utilized functional AuNPs to quantify cellular uptake and compare nanoparticle stability in different organs and suborgans using laser ablation inductively coupled plasma mass spectrometry (LA-ICP-MS) and LDI-MS imaging (Fig. 10B).^{166–169} Apart from cellular process exploration, this “mass barcode” nanoprobe was gradually applied in the sensitive detection of DNA, proteins and glycan by co-decorating with specific affinity ligands. Huang *et al.* developed a three-component sandwich structured assay composed of a capture strand decorated silicon wafer, target-DNA strands and probe-DNA strands and small alkanethiol molecule-codecorated

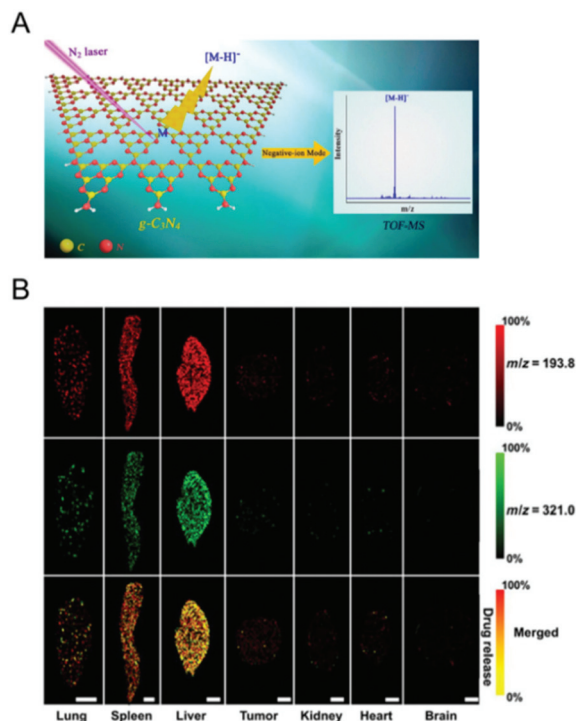


Fig. 9 (A) Using g-C₃N₄ nanosheets as the matrix for LDI-MS analysis of small molecules. Reprinted with permission from ref. 159. Copyright (2015) American Chemical Society. (B) LDI-MS image of the biodistribution of DOX/PEG-MoS₂ nanosheets in tissues of H22 tumor model mice. Reprinted with permission from ref. 161. Copyright (2018) Science.

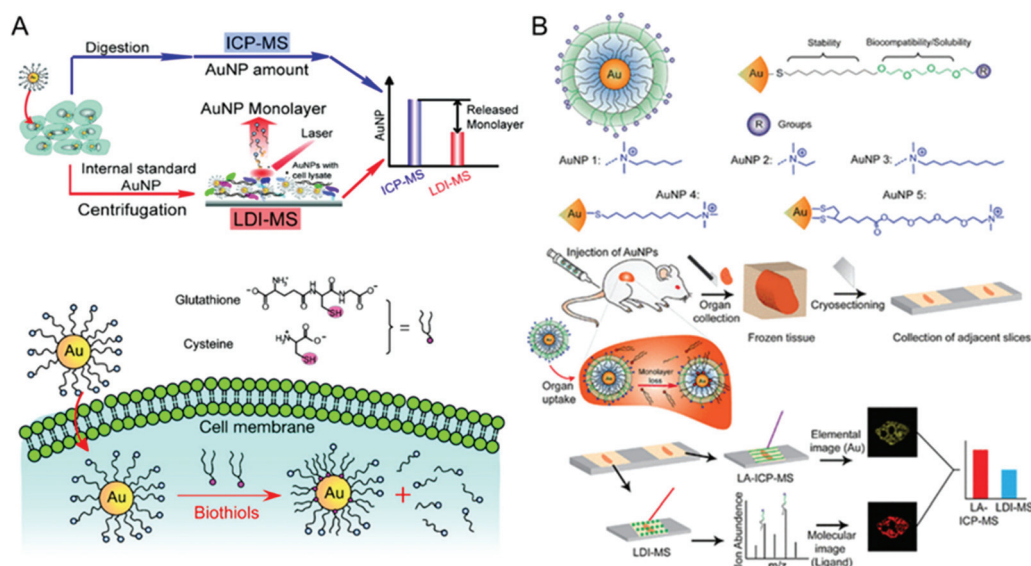


Fig. 10 (A) The approach used to measure total AuNP uptake and monolayer amounts upon exposure to cells. The difference between the values obtained by ICP MS and LDI-MS represents the amount of monolayer released from the AuNPs. Reprinted with permission from ref. 165. Copyright (2012) American Chemical Society. (B) Schematic representation of the dual-mode mass spectrometric imaging for the determination of *in vivo* stability of nanoparticle monolayers. Reprinted with permission from ref. 166. Copyright (2017) American Chemical Society.

AuNPs.¹⁷⁰ By incubation with different concentrations of target strands, functional AuNPs could be linked onto this substrate by DNA hybridization, which was further transferred to amplified ion signals of the mass barcodes on AuNPs by LDI-MS analysis, thus achieving a sensitive assay for the target DNA with a detection limit of 100 pM. Liu *et al.* used mass tag-modified AuNPs as amplifiers to profile three protein biomarkers including epithelial cell adhesion molecule (EPCAM), cytokeratin 19 (CK19) and mucin 1 protein (MUC-1) on the surface of MCF-7 cells, respectively.¹⁷¹ Three specific antibodies strengthened the affinity to target proteins and excess mass tags ensured sensitive detection. Based on a similar strategy, the accurate diagnosis of cancer at the subtype level was achieved by mass spectrometry imaging of relevant mass tags, indicative of three protein biomarkers on the surface of exosomes (Fig. 11A).¹⁷² They also identified other protein markers and multiple IgE Abs using immunomagnetic beads as capture probes and various functional AuNPs as signal converters.^{173,174} In addition, these mass tag decorated nanoprobes were also utilized for *in situ* multiplexed glycan detection and imaging.¹⁷⁵ Our group developed protease-responsive mass barcoded nanotranslators (PRMNTs) with a core-satellite structure for assaying intracellular cascaded caspases in cell apoptosis. The activities of multiple caspases could be translated into decreased ion signals of mass tags on the remaining AuNPs in the PRMNTs by MS decoding, thus achieving the quantification of the intracellular activity of caspase-3, -8, and -9 and kinetic analysis of apoptosis-inducing efficiency of various drugs.¹⁷⁶

By virtue of high desorption efficiency and low economic cost, some small molecules were also suitable candidates for mass barcodes grafted on AuNPs. The Liu group synthesized a

series of analogous rhodamine-based mass tags including RMT443, RMT415 and RMT387 for the multiplexed quantification of cell surface proteins through two-stage signal amplification in ambient mass spectrometry analysis.¹⁷⁷ The efficient dissociation of RMTs from AuNPs achieved primary amplification and in-source collision-induced dissociation (CID) provided the secondary signal amplification, thus exhibiting zeptomole detection sensitivity and multiplex quantification of three protein biomarkers. Recently, they combined the same nanoprobes with a microfluidic chip capable of dispersing and ordering cells for the semi-quantification of cell surface proteins and compatibility of endogenous metabolite detection at the single-cell level (Fig. 11B).¹⁷⁸ The homologous RMTs with two stage signal amplification ability ensured single-cell-protein sensitivity and high throughput, and meanwhile cellular metabolites could be profiled during nanoESI MS analysis. In this manner, six cell surface antigens and ~100 metabolites in ovarian cancer cell types and breast cancer cells were monitored simultaneously. Besides short polyethylene glycol compounds and small molecules, DNA fragments, peptides and lipids were also applied to construct amplification systems for probing target molecules. Cooks *et al.* have demonstrated the ability of peptide tag-decorated magnetic cluster nanoparticles for the selective capture and identification of circulating tumor cells.¹⁷⁹ The peptide-based mass encoding strategy provided an easily synthesized portfolio of molecules for multiplex quantification of analytes, from which ion signals were acquired by the detection of released peptide fragments with the assistance of protease or chemical cleavage reagents.

Zhu *et al.* also utilized plasmid-encoded peptide tags as barcode molecules for the identification of target DNA.¹⁸⁰ A unique advantage of using DNA fragments as mass barcodes is

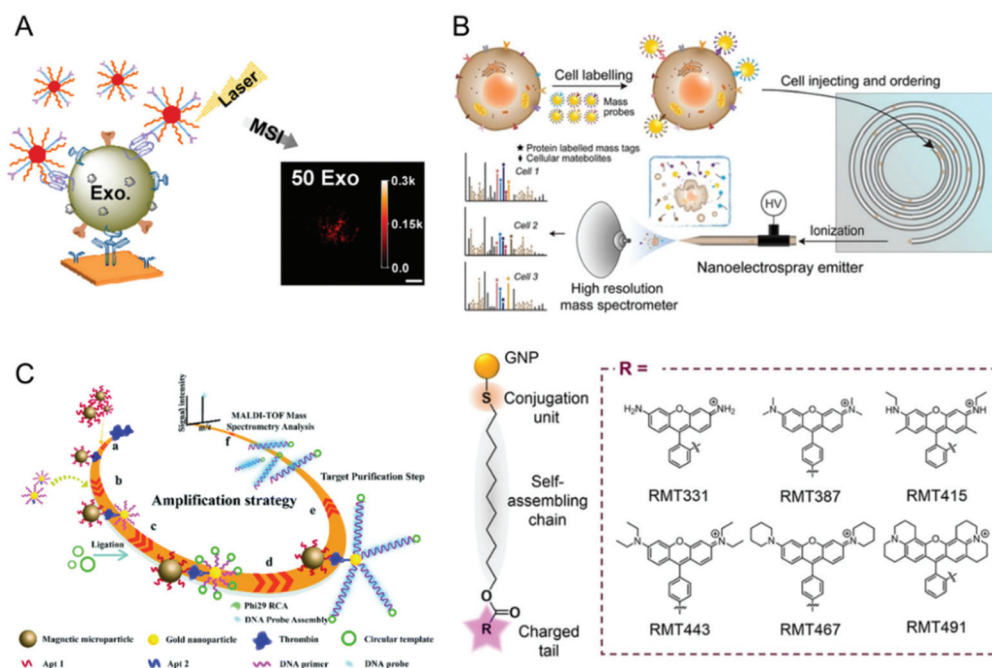


Fig. 11 (A) MS imaging of the mass tag immunoassay for quantitative profiling of biomarkers from exosomes. Reprinted with permission from ref. 172. Copyright (2021) American Chemical Society. (B) Schematic of the multi-dimensional chip-nanoESI ionization (Chip-nanoESI) organic mass cytometry and its workflow for single-cell analysis. Reprinted with permission from ref. 178. Copyright (2021) Wiley-VCH. (C) Schematic illustration of the MS signal amplification strategy: (a and b) thrombin recognition, (c and d) signal amplification, (e) purification, and (f) MALDI-TOF MS detection. Reprinted with permission from ref. 182. Copyright (2018) Royal Society of Chemistry.

that it can improve the detection sensitivity by combination with various DNA amplification techniques. The Lin group developed a DNA-mediated cell surface glycan imaging strategy, in which lectins were encoded with DNA primers, participating in subsequent rolling circle amplification (RCA) and producing repetitive single-strand DNA sequences to hybridize with complementary short DNA probes.¹⁸¹ Upon laser irradiation, the hydrogen bonds in DNA duplexes were broken and the short DNA probes were released, thus providing abundant mass barcode signals for glycan analysis. Subsequently, they also grafted the same DNA-mediated RCA amplification strategy onto a sandwich structured assay composed of magnetic nanoparticles and AuNPs with specific affinity to thrombin (Fig. 11C).¹⁸² Other DNA decorated amplification assays were also developed for multiplexed analysis of biomolecules including proteins and DNA molecules.¹⁸³ Jiang *et al.* reported a multiplexed protein detection method by adopting phospholipids with different molecular weights as the encoded MS reporters.¹⁸⁴ Phospholipids could be non-covalently coated onto AuNPs *via* a simple self-assembly procedure, which enabled efficient ionization without breaking the covalent bonds to achieve sensitive analysis.

4.2 Metal clusters of nanoprobe as the signal output

Apart from denoting surface ligands on metal nanoprobe as amplified mass reporters, abundant metal cluster peaks observed under laser irradiation inspired researchers to

develop an amplification strategy by utilizing the metal cluster ion signals. The Huang group was devoted to developing a series of LDI-MS quantification strategies using Au-cluster ions as substitute ion signals for the detection of metal ions, proteins and cells.^{185–192} They selected BSA-modified AuNPs as the LDI matrix, which could be trapped by nitrocellulose membranes (NCMs) due to strong hydrophobic interactions. Upon addition of Pb^{2+} ions, $Au^+ \cdot S_2O_3^{2-}$ complexes could adsorb the Pb^{2+} to form Au–Pb ions for MS determination of the Pb^{2+} concentration (Fig. 12A).¹⁸⁵ Furthermore, they also assayed I^- and AsO_2^- in the same detection manner.^{186,187} Taking advantage of the traditional sandwich structured immunoassay, they also profiled viral infections *via* Au cluster signals from coupled AuNPs.¹⁸⁸ On the other hand, the decentralized states and surface coverage of AuNPs also have an impact on the D/I efficiency of Au atoms from the AuNP surface. Based on this, they continued their research on measuring circulating tumor cells and thrombin by the decreased Au cluster signals arising from less exposed surfaces due to blocking by cells or proteins.^{189,190} Besides, they synthesized AuNP-modified cellulose ester membranes (MCEMs) to monitor thrombin generation. When thrombin reacted with fibrinogen, insoluble fibrin was formed, hindering the formation of Au clusters and decreasing the signal intensity. This approach allowed the detection of thrombin (limit of detection of *ca.* 2.5 pM) in human plasma samples.¹⁹¹ They also took advantage of the same MCEM platform to detect the activity of plasmin by inter-

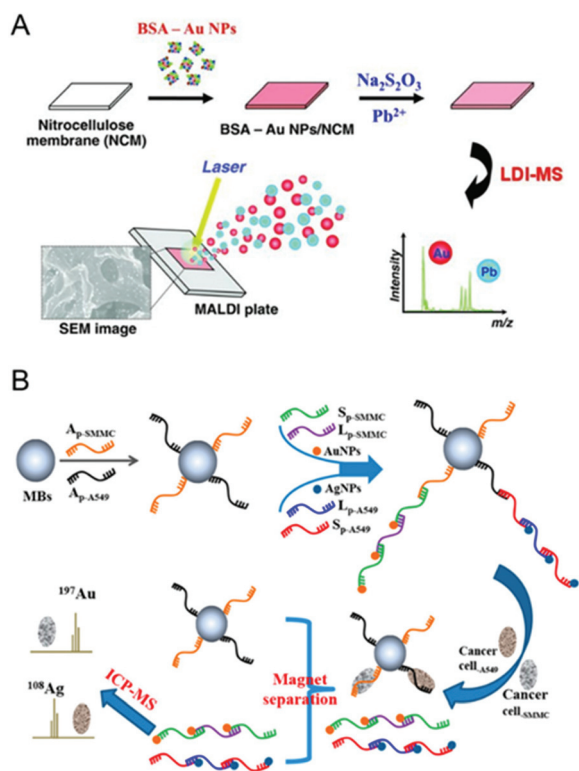


Fig. 12 (A) Schematic representation of the preparation of the BSA-AuNP/NCM nanocomposite and its use for the analysis of Pb^{2+} ions through LDI-MS. Reprinted with permission from ref. 185. Copyright (2011) Wiley-VCH. (B) Schematic illustration of the experimental principle for simultaneously counting SMMC-7721 and A549 cells based on ICP-MS and the MBs-based dual aptamer-dual metal nanoparticle labeling technique. Reprinted with permission from ref. 195. Copyright (2019) American Chemical Society.

preparing the decreased Au cluster signals from agglutinative Fib-AuNPs.¹⁹²

Apart from the LDI analysis of metal cluster ions, the inductively coupled mass spectrometry (ICP-MS) based element-tagged strategy also demonstrated its ultra-sensitive detection ability in biomolecule analysis. Hu *et al.* reported a sensitive immunoassay protocol for the detection of tumor cells by using ICP-MS with two nanoprobables.¹⁹³ In this method, immunomagnetic beads and antibody-functionalized AuNPs were both linked with cells, thus achieving fast magnetic separation and amplified detection after ICP-MS based quantification of the Au content. Wang *et al.* developed a silver nanocluster-based ICP-MS amplification strategy to profile the activity of alkaline phosphatase (ALP).¹⁹⁴ Up-conversion nanoparticles (UCNPs) and silver nanoclusters (AgNCs) were formatted in a core-satellite structure with a DNA linker. This core-satellite structure was destroyed by alkaline phosphatase mediated dephosphorylation of the DNA linker, which weakened the coordination of DNA with UCNPs and accelerated the shedding of AgNCs. ICP-MS quantification of the liberated Ag content ensured favorable sensitivity for ALP activity assay. Fu *et al.* combined the magnetic-bead-based multiplexed metal nano-

particle labeling technique and hybridization chain reaction amplification for simultaneous recognition of multiple cancer cells.¹⁹⁵ Multiple aptamer-functionalized magnetic beads (MBs) were applied in cell recognition and convenient separation, and the AuNP and AgNP labeling involved in the HCR amplification assay ensured ICP MS signal generation, resulting in a limit of detection as low as 50 SMMC-7721 and A549 cancer cells in serum (Fig. 12B). Taking advantage of the fluorescence characteristics of Au clusters, the Gao group directly observed membrane type-1 matrix metalloproteinase (MT1-MMP) *via* fluorescence microscopy and quantitatively profiled the MT1-MMP expression by inductively coupled plasma mass spectrometry 2D mapping of the Au element.¹⁹⁶ By comparing the MT1-MMP expression levels in primary human lung carcinoma and human renal carcinoma tissue sections, they successfully assessed the risk of primary tumor invasion. More recently, Au_{26} clusters and Ag_{12} clusters were respectively employed to encode MT1-MMP and integrin $\alpha_v\beta_3$ proteins for synchronous quantification of the two proteins.¹⁹⁷ In addition to the metal nanoparticle labelling strategy, a series of lanthanide-doped nanoparticles were also developed by making use of the affluent library of lanthanides in nature for the multiplex quantification assay and biodistribution evaluation of nanoparticles.^{198,199}

5. Conclusions and outlook

In summary, we have reviewed the advances in the engineering of nanomaterials towards facilitating sensitive MS analysis of biomolecules, which can be divided into three aspects according to the different functions: sample pre-treatment for target biomolecule enrichment prior to MS analysis, enhancement of the desorption/ionization of analytes during MS interrogation and signal amplification to improve the MS readout. In the pre-treatment process, different compositions and characteristics of nanomaterials have a great influence on the enrichment specificity towards endogenous peptides, phosphopeptides and glycopeptides, while surface functionalization or multi-component combination also exerts a synergistic effect on further improving the capture efficiency.

First, nanomaterials featuring size-exclusive properties and hydrophobic surfaces showed outstanding selectivity and efficiency in the enrichment of ordinary peptides. For phosphopeptide enrichment, the developments of Zr(IV) and Ti(IV) containing IMAC/MOAC nanomaterials dominated efforts in the engineering of bioaffinity nanostructures, and the construction of hybrid nanomaterials and integration of multiple chelators further improved the enrichment performance. Thirdly, lectin-based affinity, hydrophilic-hydrophilic interactions and covalent interactions are three major strategies for the harvest of glycopeptides by using nanomaterials, among which boronic acid functionalized materials attract increasing attention nowadays due to their superior specificity and simple enrichment process.

In the D/I process, various types of nanomaterials such as silicon-based nanomaterials, carbon-based nanomaterials, metal nanoparticles, metal oxides and MOFs, proved their unique advantages in MS imaging and analysis of biomolecules compared to organic matrices. Both ordered silicon arrays and heteroatom doping on carbon-based nanomaterials contribute to the D/I process of analytes. Besides, some semi-conductive metal oxides, such as TiO₂ and ZnO, were found to have high photoreactivity and unique electron-transfer capacity to accelerate the desorption/ionization. Although MOFs and other 2D nanomaterials also presented satisfactory performance in the detection of small molecules, more surface functionalization strategies or in-depth applications need to be explored.

Recently, various metal nanoparticles have been widely applied in the ultrasensitive detection of biomolecules and cellular uptake analysis by MS decoding of surface ligands or metal clusters. Up to now, a series of surface ligands, including short polyethylene glycol compounds, short-chain DNA molecules, peptides and lipids, have been adopted as the coating ligands of nanoparticles and also mass reporters for reflecting the entity and amount of target biomolecules. On the other hand, engineering of diverse metal nanoparticles has been successfully involved in various biosensing systems by delivering metal cluster signals upon LDI-MS or ICP-MS analysis.

Although great efforts have been made in developing functional nanomaterials for improving the MS readout of biomolecules, it is still far from ideal and more attention needs to be focused on the innovation of nanomaterials and exploitation of in-depth applications. (1) From the materials side, more tailored nanomaterials with multiple functions and higher affinity and specificity need to be developed to meet the increasing analytical requirements for large-scale identification of multiple targets in complex bio-samples. For example, more efforts should be devoted to the vigorous development of nanomaterials that can synchronously capture peptides or proteins with multi-PTM to achieve satisfactory depth and coverage of proteomes. Besides, although some nanomaterials have been developed to simultaneously separate and detect the targets, the enrichment capacity and desorption/ionization efficiency need to be further improved. (2) For the mechanism investigation, much attention should be continuously directed to unveil the underlying relationship between the structure of nanomaterials and the desorption/ionization efficiency of analytes, which may provide guidance to purposefully customize nanomaterials with high energy absorption and transfer capacity, and low background interferences in MS analysis. (3) From the viewpoint of application, the use of nanomaterials in MS characterization should aim to address the unique characterization challenges inaccessible to other methodologies. One example is to devise nanoprobe that can monitor endogenous biomarker metabolites or exogenous therapeutic agent release in tissues by MS imaging of their molecular weight signals or alternative mass tag signals. In addition, MS can also be combined with complementary

detection modalities with diverse technical advantages. For instance, developing multimodal methodologies that combine MS with Raman spectroscopy, fluorescence or other analytical techniques can maximize the effective information extracted from complex samples to address the crucial needs and challenges in clinical diagnosis.

Conflicts of interest

There are no conflicts to declare.

Acknowledgements

The authors are grateful for the financial support from the National Natural Science Foundation of China (No. 21974062, 92053102), the Fundamental Research Funds for the Central Universities (020514380255), and the State Key Laboratory of Analytical Chemistry for Life Science (SKLACLS2107).

References

- 1 B. Domon and R. Aebersold, *Science*, 2006, **312**, 212.
- 2 K. Shibamoto, K. Sakata, K. Nagoshi and T. Korenaga, *J. Phys. Chem. C*, 2009, **113**, 17774–17779.
- 3 R. W. Nelson, D. Dogruel, P. Williams and R. Beavis, *Rapid Commun. Mass Spectrom.*, 1994, **8**, 627–631.
- 4 N. Sun, H. Wu, X. Shen and C. Deng, *Adv. Funct. Mater.*, 2019, **29**, 1900253.
- 5 A. Y. Lim, J. Ma and Y. C. F. Boey, *Adv. Mater.*, 2012, **24**, 4211–4216.
- 6 M. Karas, D. Bachmann, U. Bahr and F. Hillenkamp, *Int. J. Mass Spectrom. Ion Processes*, 1987, **78**, 53–68.
- 7 M. Yamashita and J. B. Fenn, *J. Phys. Chem.*, 1984, **88**, 4451–4459.
- 8 Z.-G. Wang, N. Lv, W.-Z. Bi, J.-L. Zhang and J.-Z. Ni, *ACS Appl. Mater. Interfaces*, 2015, **7**, 8377–8392.
- 9 S. Suttapitugsakul, F. Sun and R. Wu, *Anal. Chem.*, 2020, **92**, 267–291.
- 10 J. Peng, H. Zhang, H. Niu and R. A. Wu, *TrAC, Trends Anal. Chem.*, 2020, **125**, 115835.
- 11 D. S. Peterson, *Mass Spectrom. Rev.*, 2007, **26**, 19–34.
- 12 C.-K. Chiang, M.-C. Chiang, Z.-H. Lin, G.-Y. Lan, Y.-W. Lin and H.-T. Chang, *J. Am. Soc. Mass Spectrom.*, 2010, **21**, 1204–1207.
- 13 C.-K. Chiang, W.-T. Chen and H.-T. Chang, *Chem. Soc. Rev.*, 2011, **40**, 1269–1281.
- 14 H. Qin, P. Gao, F. Wang, L. Zhao, J. Zhu, A. Wang, T. Zhang, R. A. Wu and H. Zou, *Angew. Chem., Int. Ed.*, 2011, **50**, 12218–12221.
- 15 Q. Chen, M.-M. Wang, X. Hu, X.-W. Chen and J.-H. Wang, *J. Mater. Chem. B*, 2016, **4**, 6812–6819.
- 16 L. Chen, J. Ou, H. Wang, Z. Liu, M. Ye and H. Zou, *ACS Appl. Mater. Interfaces*, 2016, **8**, 20292–20300.

- 17 B. Luo, M. Yang, P. Jiang, F. Lan and Y. Wu, *Nanoscale*, 2018, **10**, 8391–8396.
- 18 G. Qing, Q. Lu, X. Li, J. Liu, M. Ye, X. Liang and T. Sun, *Nat. Commun.*, 2017, **8**, 461.
- 19 R. Pilolli, F. Palmisano and N. Cioffi, *Anal. Bioanal. Chem.*, 2012, **402**, 601–623.
- 20 H. N. Abdelhamid, *Microchim. Acta*, 2019, **186**, 682.
- 21 S. Chen, C. Xiong, H. Liu, Q. Wan, J. Hou, Q. He, A. Badu-Tawiah and Z. Nie, *Nat. Nanotechnol.*, 2015, **10**, 176–182.
- 22 L. Qiao, B. Liu and H. H. Girault, *Nanomedicine*, 2010, **5**, 1641–1652.
- 23 A. D. Tinoco and A. Saghatelian, *Biochemistry*, 2011, **50**, 7447–7461.
- 24 D. C. Rubinsztein, *Nature*, 2006, **443**, 780–786.
- 25 P. Bastos, F. Trindade, R. Ferreira, M. A. Casteleiro, R. Stevens, J. Klein and R. Vitorino, *J. Proteomics*, 2018, **171**, 53–62.
- 26 P. D. Rakowska and M. G. Ryadnov, *Biomarkers Med.*, 2011, **5**, 387–396.
- 27 R. Tian, L. Ren, H. Ma, X. Li, L. Hu, M. Ye, R. A. Wu, Z. Tian, Z. Liu and H. Zou, *J. Chromatogr. A*, 2009, **1216**, 1270–1278.
- 28 R. Tian, H. Zhang, M. Ye, X. Jiang, L. Hu, X. Li, X. Bao and H. Zou, *Angew. Chem., Int. Ed.*, 2007, **119**, 980–983.
- 29 L. Zhang, S. Wu, C. Li and Q. Yang, *Chem. Commun.*, 2012, **48**, 4190–4192.
- 30 S. Liu, Y. Li, C. Deng, Y. Mao, X. Zhang and P. Yang, *Proteomics*, 2011, **11**, 4503–4513.
- 31 L. Hu, H. Zhou, Y. Li, S. Sun, L. Guo, M. Ye, X. Tian, J. Gu, S. Yang and H. Zou, *Anal. Chem.*, 2009, **81**, 94–104.
- 32 Q. Zhang, Z. Xiong, H. Wan, X. Chen, H. Li and H. Zou, *Talanta*, 2016, **146**, 272–278.
- 33 Y. Gan, Q. Zhang, Y. Chen, Y. Zhao, Z. Xiong, L. Zhang and W. Zhang, *Talanta*, 2016, **161**, 647–654.
- 34 M. Zhao, Y. Xie, H. Chen and C. Deng, *Talanta*, 2017, **167**, 392–397.
- 35 G. Cheng, M.-D. Zhou and S.-Y. Zheng, *ACS Appl. Mater. Interfaces*, 2014, **6**, 12719–12728.
- 36 G. Lin, C. Gao, Q. Zheng, Z. Lei, H. Geng, Z. Lin, H. Yang and Z. Cai, *Chem. Commun.*, 2017, **53**, 3649–3652.
- 37 C. Gao, G. Lin, Z. Lei, Q. Zheng, J. Lin and Z. Lin, *J. Mater. Chem. B*, 2017, **5**, 7496–7503.
- 38 W. Ma, Q. Zheng, Y. He, G. Li, W. Guo, Z. Lin and L. Zhang, *J. Am. Chem. Soc.*, 2019, **141**, 18271–18277.
- 39 J. Schlessinger, *Cell*, 2000, **103**, 211–225.
- 40 T. E. Thingholm, T. J. D. Jørgensen, O. N. Jensen and M. R. Larsen, *Nat. Protoc.*, 2006, **1**, 1929–1935.
- 41 L. Andersson and J. Porath, *Anal. Biochem.*, 1986, **154**, 250–254.
- 42 Y. Li, Y. Liu, J. Tang, H. Lin, N. Yao, X. Shen, C. Deng, P. Yang and X. Zhang, *J. Chromatogr. A*, 2007, **1172**, 57–71.
- 43 Y. Yan and C. Deng, *TrAC, Trends Anal. Chem.*, 2019, **120**, 115655.
- 44 Y. Hong, H. Zhao, C. Pu, Q. Zhan, Q. Sheng and M. Lan, *Anal. Chem.*, 2018, **90**, 11008–11015.
- 45 J. Su, X. He, L. Chen and Y. Zhang, *ACS Sustainable Chem. Eng.*, 2018, **6**, 2188–2196.
- 46 Y. Hong, Y. Yao, H. Zhao, Q. Sheng, M. Ye, C. Yu and M. Lan, *Anal. Chem.*, 2018, **90**, 7617–7625.
- 47 Y. Yan, Z. Zheng, C. Deng, Y. Li, X. Zhang and P. Yang, *Anal. Chem.*, 2013, **85**, 8483–8487.
- 48 Y. Yan, Z. Zheng, C. Deng, X. Zhang and P. Yang, *Chem. Commun.*, 2013, **49**, 5055–5057.
- 49 C. Shi, Q. Lin and C. Deng, *Talanta*, 2015, **135**, 81–86.
- 50 P. L. Stanghellini, E. Boccaleri, E. Diana, G. Alberti and R. Vivani, *Inorg. Chem.*, 2004, **43**, 5698–5703.
- 51 L. Zhao, H. Qin, Z. Hu, Y. Zhang, R. A. Wu and H. Zou, *Chem. Sci.*, 2012, **3**, 2828.
- 52 Y. Yan, X. Sun, C. Deng, Y. Li and X. Zhang, *Anal. Chem.*, 2014, **86**, 4327–4332.
- 53 W. Li, Q. Deng, G. Fang, Y. Chen, J. Zhan and S. Wang, *J. Mater. Chem. B*, 2013, **1**, 1947–1961.
- 54 G. Fang, W. Gao, Q. Deng, K. Qian, H. Han and S. Wang, *Anal. Biochem.*, 2012, **423**, 210–217.
- 55 Y. Yan, X. Zhang and C. Deng, *ACS Appl. Mater. Interfaces*, 2014, **6**, 5467–5471.
- 56 Q. Min, S. Li, X. Chen, E. S. Abdel-Halim, L.-P. Jiang and J.-J. Zhu, *ACS Appl. Mater. Interfaces*, 2015, **7**, 9563–9572.
- 57 H. Xu, M. Liu, X. Huang, Q. Min and J.-J. Zhu, *Anal. Chem.*, 2018, **90**, 9859–9867.
- 58 X. Qi, L. Chen, C. Zhang, X. Xu, Y. Zhang, Y. Bai and H. Liu, *ACS Appl. Mater. Interfaces*, 2016, **8**, 18675–18683.
- 59 X.-Y. Long, Z.-J. Zhang, J.-Y. Li, D. Sheng and H.-Z. Lian, *Anal. Chem.*, 2017, **89**, 10446–10453.
- 60 C. B. Messner, M. R. Mirza, M. Rainer, O. M. D. Lutz, Y. Güzel, T. S. Hofer, C. W. Huck, B. M. Rode and G. K. Bonn, *Anal. Methods*, 2013, **5**, 2379–2383.
- 61 X. Zhu, J. Gu, J. Yang, Z. Wang, Y. Li, L. Zhao, W. Zhao and J. Shi, *J. Mater. Chem. B*, 2015, **3**, 4242–4248.
- 62 Y. Chen, Z. Xiong, L. Peng, Y. Gan, Y. Zhao, J. Shen, J. Qian, L. Zhang and W. Zhang, *ACS Appl. Mater. Interfaces*, 2015, **7**, 16338–16347.
- 63 L.-N. Xu, L.-P. Li, L. Jin, Y. Bai and H.-W. Liu, *Chem. Commun.*, 2014, **50**, 10963–10966.
- 64 Z. Xiong, Y. Chen, L. Zhang, J. Ren, Q. Zhang, M. Ye, W. Zhang and H. Zou, *ACS Appl. Mater. Interfaces*, 2014, **6**, 22743–22750.
- 65 A. Helenius and M. Aebi, *Science*, 2001, **291**, 2364.
- 66 Y. Yang, V. Franc and A. J. R. Heck, *Trends Biotechnol.*, 2017, **35**, 598–609.
- 67 E. Song, R. Zhu, Z. T. Hammoud and Y. Mechref, *J. Proteome Res.*, 2014, **13**, 4808–4820.
- 68 K. Wang, E. D. Peng, A. S. Huang, D. Xia, S. J. Vermont, G. Lentini, M. Lebrun, J. M. Wastling and P. J. Bradley, *PLoS One*, 2016, **11**, e0150561.
- 69 L. Dong, S. Feng, S. Li, P. Song and J. Wang, *Anal. Chem.*, 2015, **87**, 6849–6853.
- 70 J. A. Ferreira, A. L. Daniel-da-Silva, R. M. P. Alves, D. Duarte, I. Vieira, L. L. Santos, R. Vitorino and F. Amado, *Anal. Chem.*, 2011, **83**, 7035–7043.

- 71 S. M. Totten, C. L. Feasley, A. Bermudez and S. J. Pitteri, *J. Proteome Res.*, 2017, **16**, 1249–1260.
- 72 P. Kozlik, M. Sanda and R. Goldman, *J. Chromatogr. A*, 2017, **1519**, 152–155.
- 73 Y. Li, J. Wang, N. Sun and C.-H. Deng, *Anal. Chem.*, 2017, **89**, 11151–11158.
- 74 W. Ma, L. Xu, Z. Li, Y. Sun, Y. Bai and H. Liu, *Nanoscale*, 2016, **8**, 10908–10912.
- 75 S. I. Snovida, E. D. Bodnar, R. Viner, J. Saba and H. Perreault, *Carbohydr. Res.*, 2010, **345**, 792–801.
- 76 Y. Chen, Q. Sheng, Y. Hong and M. Lan, *Anal. Chem.*, 2019, **91**, 4047–4054.
- 77 H. Bai, C. Fan, W. Zhang, Y. Pan, L. Ma, W. Ying, J. Wang, Y. Deng, X. Qian and W. Qin, *Chem. Sci.*, 2015, **6**, 4234–4241.
- 78 Y. Xie, Q. Liu, Y. Li and C. Deng, *J. Chromatogr. A*, 2018, **1540**, 87–93.
- 79 X. Zhang, J. Wang, X. He, L. Chen and Y. Zhang, *ACS Appl. Mater. Interfaces*, 2015, **7**, 24576–24584.
- 80 Y. Wang, M. Liu, L. Xie, C. Fang, H. Xiong and H. Lu, *Anal. Chem.*, 2014, **86**, 2057–2064.
- 81 J. Yao, J. Wang, N. Sun and C. Deng, *Nanoscale*, 2017, **9**, 16024–16029.
- 82 B. Jiang, Y. Qu, L. Zhang, Z. Liang and Y. Zhang, *Anal. Chim. Acta*, 2016, **912**, 41–48.
- 83 X. Zhang, J. Wang, X. He, L. Chen and Y. Zhang, *ACS Appl. Mater. Interfaces*, 2015, **7**, 24576–24584.
- 84 H. Xiao, W. Chen, J. M. Smeeckens and R. Wu, *Nat. Commun.*, 2018, **9**, 1692.
- 85 M. Lu, X. Yang, Y. Yang, P. Qin, X. Wu and Z. Cai, *Nanomaterials*, 2017, **7**, 87.
- 86 H. He, Z. Guo, Y. Wen, S. Xu and Z. Liu, *Anal. Chim. Acta*, 2019, **1090**, 1–22.
- 87 H. N. Abdelhamid, *Microchim. Acta*, 2018, **185**, 200.
- 88 L. Huang, J. Wan, X. Wei, Y. Liu, J. Huang, X. Sun, R. Zhang, D. D. Gurav, V. Vedarethinam, Y. Li, R. Chen and K. Qian, *Nat. Commun.*, 2017, **8**, 220.
- 89 H. Nasser Abdelhamid, B.-S. Wu and H.-F. Wu, *Talanta*, 2014, **126**, 27–37.
- 90 S. K. Kailasa and H.-F. Wu, *Anal. Bioanal. Chem.*, 2010, **396**, 1115–1125.
- 91 J. Wei, J. M. Buriak and G. Siuzdak, *Nature*, 1999, **399**, 243–246.
- 92 T. Guinan, C. Della Vedova, H. Kobus and N. H. Voelcker, *Chem. Commun.*, 2015, **51**, 6088–6091.
- 93 T. M. Guinan, H. Abdelmaksoud and N. H. Voelcker, *Chem. Commun.*, 2017, **53**, 5224–5226.
- 94 E. P. Go, J. V. Apon, G. Luo, A. Saghatelian, R. H. Daniels, V. Sahi, R. Dubrow, B. F. Cravatt, A. Vertes and G. Siuzdak, *Anal. Chem.*, 2005, **77**, 1641–1646.
- 95 X. Chen, T. Wang, L. Lin, F. Wo, Y. Liu, X. Liang, H. Ye and J. Wu, *ACS Appl. Mater. Interfaces*, 2018, **10**, 14389–14398.
- 96 D. Brodoceanu, R. Elnathan, B. Prieto-Simón, B. Delalat, T. Guinan, E. Kroner, N. H. Voelcker and T. Kraus, *ACS Appl. Mater. Interfaces*, 2015, **7**, 1160–1169.
- 97 B. N. Walker, T. Razunguzwa, M. Powell, R. Knochenmuss and A. Vertes, *Angew. Chem., Int. Ed.*, 2009, **48**, 1669–1672.
- 98 B. N. Walker, C. Antonakos, S. T. Retterer and A. Vertes, *Angew. Chem., Int. Ed.*, 2013, **52**, 3650–3653.
- 99 A. R. Korte, S. A. Stopka, N. Morris, T. Razunguzwa and A. Vertes, *Anal. Chem.*, 2016, **88**, 8989–8996.
- 100 L. Z. Samarah, T. H. Tran, G. Stacey and A. Vertes, *Angew. Chem., Int. Ed.*, 2021, **60**, 9071–9077.
- 101 T. Guinan, C. Della Vedova, H. Kobus and N. H. Voelcker, *Chem. Commun.*, 2015, **51**, 6088–6091.
- 102 M. Ronci, D. Rudd, T. Guinan, K. Benkendorff and N. H. Voelcker, *Anal. Chem.*, 2012, **84**, 8996–9001.
- 103 J. Sunner, E. Dratz and Y.-C. Chen, *Anal. Chem.*, 1995, **67**, 4335–4342.
- 104 H. N. Abdelhamid and H.-F. Wu, *Analyst*, 2015, **140**, 1555–1565.
- 105 Y.-K. Kim and D.-H. Min, *ACS Appl. Mater. Interfaces*, 2012, **4**, 2088–2095.
- 106 Q. Min, X. Zhang, X. Chen, S. Li and J.-J. Zhu, *Anal. Chem.*, 2014, **86**, 9122–9130.
- 107 H.-W. Tang, K.-M. Ng, W. Lu and C.-M. Che, *Anal. Chem.*, 2009, **81**, 4720–4729.
- 108 S. Xu, Y. Li, H. Zou, J. Qiu, Z. Guo and B. Guo, *Anal. Chem.*, 2003, **75**, 6191–6195.
- 109 S.-F. Ren and Y.-L. Guo, *Rapid Commun. Mass Spectrom.*, 2005, **19**, 255–260.
- 110 M. Najam-ul-Haq, M. Rainer, T. Schwarzenauer, C. W. Huck and G. K. Bonn, *Anal. Chim. Acta*, 2006, **561**, 32–39.
- 111 J. Lee, Y.-K. Kim and D.-H. Min, *J. Am. Chem. Soc.*, 2010, **132**, 14714–14717.
- 112 Y. Yan, Z. Zheng, C. Deng, X. Zhang and P. Yang, *Talanta*, 2014, **118**, 14–20.
- 113 X.-S. Li, J.-H. Wu, L.-D. Xu, Q. Zhao, Y.-B. Luo, B.-F. Yuan and Y.-Q. Feng, *Chem. Commun.*, 2011, **47**, 9816–9818.
- 114 J. Wang, M. Cheng, Z. Zhang, L. Guo, Q. Liu and G. Jiang, *Chem. Commun.*, 2015, **51**, 4619–4622.
- 115 X. Huang, Q. Liu, X. Huang, Z. Nie, T. Ruan, Y. Du and G. Jiang, *Anal. Chem.*, 2017, **89**, 1307–1314.
- 116 D. Wang, X. Huang, J. Li, B. He, Q. Liu, L. Hu and G. Jiang, *Chem. Commun.*, 2018, **54**, 2723–2726.
- 117 H. Zhao, Y. Li, J. Wang, M. Cheng, Z. Zhao, H. Zhang, C. Wang, J. Wang, Y. Qiao and J. Wang, *ACS Appl. Mater. Interfaces*, 2018, **10**, 37732–37742.
- 118 S. Chen, H. Zheng, J. Wang, J. Hou, Q. He, H. Liu, C. Xiong, X. Kong and Z. Nie, *Anal. Chem.*, 2013, **85**, 6646–6652.
- 119 S. Chen, C. Xiong, H. Liu, Q. Wan, J. Hou, Q. He, A. Badu-Tawiah and Z. Nie, *Nat. Nanotechnol.*, 2015, **10**, 176–182.
- 120 W. Lu, Y. Li, R. Li, S. Shuang, C. Dong and Z. Cai, *ACS Appl. Mater. Interfaces*, 2016, **8**, 12976–12984.
- 121 Z. Lin, J. Wu, Y. Dong, P. Xie, Y. Zhang and Z. Cai, *Anal. Chem.*, 2018, **90**, 10872–10880.
- 122 J. A. McLean, K. A. Stumpo and D. H. Russell, *J. Am. Chem. Soc.*, 2005, **127**, 5304–5305.

- 123 Y.-C. Liu, Y.-J. Li and C.-C. Huang, *Anal. Chem.*, 2013, **85**, 1021–1028.
- 124 H. Kawasaki, T. Ozawa, H. Hisatomi and R. Arakawa, *Rapid Commun. Mass Spectrom.*, 2012, **26**, 1849–1858.
- 125 T.-R. Kuo, Y.-C. Chen, C.-I. Wang, T.-H. Shen, H.-Y. Wang, X.-Y. Pan, D.-Y. Wang, C.-C. Liou, Y.-H. Chang, Y.-C. Chen, Y.-H. Wu, Y.-R. Liu, Y.-H. Lin, C.-C. Hu and C.-C. Chen, *Nanoscale*, 2017, **9**, 11119–11125.
- 126 X. Wei, Z. Liu, X. Jin, L. Huang, D. D. Gurav, X. Sun, B. Liu, J. Ye and K. Qian, *Anal. Chim. Acta*, 2017, **950**, 147–155.
- 127 F. Ding, Y. Qian, Z. Deng, J. Zhang, Y. Zhou, L. Yang, F. Wang, J. Wang, Z. Zhou and J. Shen, *Nanoscale*, 2018, **10**, 22044–22054.
- 128 M. E. Kurczy, Z.-J. Zhu, J. Ivanisevic, A. M. Schuyler, K. Lalwani, A. F. Santidrian, J. M. David, A. Giddabasappa, A. J. Roberts, H. J. Olivos, P. J. O'Brien, L. Franco, M. W. Fields, L. P. Paris, M. Friedlander, C. H. Johnson, A. A. Epstein, H. E. Gendelman, M. R. Wood, B. H. Felding, G. J. Patti, M. E. Spilker and G. Siuzdak, *Nat. Commun.*, 2015, **6**, 5998.
- 129 A. Palermo, E. M. Forsberg, B. Warth, A. E. Aisporna, E. Billings, E. Kuang, H. P. Benton, D. Berry and G. Siuzdak, *ACS Nano*, 2018, **12**, 6938–6948.
- 130 M. Guan, Z. Zhang, S. Li, J. A. Liu, L. Liu, H. Yang, Y. Zhang, T. Wang and Z. Zhao, *Talanta*, 2018, **179**, 624–631.
- 131 T. M. Guinan, O. J. R. Gustafsson, G. McPhee, H. Kobus and N. H. Voelcker, *Anal. Chem.*, 2015, **87**, 11195–11202.
- 132 Y.-H. Cheng, Y. Zhang, S.-L. Chau, S. K.-M. Lai, H.-W. Tang and K.-M. Ng, *ACS Appl. Mater. Interfaces*, 2016, **8**, 29668–29675.
- 133 J. Yang, R. Wang, L. Huang, M. Zhang, J. Niu, C. Bao, N. Shen, M. Dai, Q. Guo, Q. Wang, Q. Wang, Q. Fu and K. Qian, *Angew. Chem., Int. Ed.*, 2020, **59**, 1703–1710.
- 134 G. Xu, S. Liu, J. Peng, W. Lv and R. A. Wu, *ACS Appl. Mater. Interfaces*, 2015, **7**, 2032–2038.
- 135 S. S. Hinman, C.-Y. Chen, J. Duan and Q. Cheng, *Nanoscale*, 2016, **8**, 1665–1675.
- 136 Y. Zhao, G. Deng, X. Liu, L. Sun, H. Li, Q. Cheng, K. Xi and D. Xu, *Anal. Chim. Acta*, 2016, **937**, 87–95.
- 137 Q. Xu, R. Tian, C. Lu and H. Li, *ACS Appl. Mater. Interfaces*, 2018, **10**, 44751–44759.
- 138 Q. Liang, J. Sherwood, T. Macher, J. M. Wilson, Y. Bao and C. J. Cassidy, *J. Am. Soc. Mass Spectrom.*, 2017, **28**, 409–418.
- 139 Q. Liang, T. Macher, Y. Xu, Y. Bao and C. J. Cassidy, *Anal. Chem.*, 2014, **86**, 8496–8503.
- 140 Y.-R. Ma, X.-L. Zhang, T. Zeng, D. Cao, Z. Zhou, W.-H. Li, H. Niu and Y.-Q. Cai, *ACS Appl. Mater. Interfaces*, 2013, **5**, 1024–1030.
- 141 M. J. Kim, J. M. Park, J. Y. Noh, T. G. Yun, M. J. Kang and J. C. Pyun, *Rapid Commun. Mass Spectrom.*, 2019, **33**, 527–538.
- 142 C.-T. Chen and Y.-C. Chen, *Anal. Chem.*, 2005, **77**, 5912–5919.
- 143 I. A. Popović, M. Nešić, M. Vranješ, Z. Šaponjić and M. Petković, *Anal. Bioanal. Chem.*, 2016, **408**, 7481–7490.
- 144 Q. Wu, J. L. Chu, S. S. Rubakhin, M. U. Gillette and J. V. Sweedler, *Chem. Sci.*, 2017, **8**, 3926–3938.
- 145 L. Qiao, C. Roussel, J. Wan, J. Kong, P. Yang, H. H. Girault and B. Liu, *Angew. Chem., Int. Ed.*, 2008, **47**, 2646–2648.
- 146 Y. Zhu, N. Gasilova, M. Jović, L. Qiao, B. Liu, L. T. Lovey, H. Pick and H. H. Girault, *Chem. Sci.*, 2018, **9**, 2212–2221.
- 147 H. Zhong, J. Zhang, X. Tang, W. Zhang, R. Jiang, R. Li, D. Chen, P. Wang and Z. Yuan, *Nat. Commun.*, 2017, **8**, 14524.
- 148 H. Zhong, J. Fu, X. Wang and S. Zheng, *Anal. Chim. Acta*, 2012, **729**, 45–53.
- 149 X. Tang, L. Huang, W. Zhang and H. Zhong, *Anal. Chem.*, 2015, **87**, 2693–2701.
- 150 G. Lu, S. Li, Z. Guo, O. K. Farha, B. G. Hauser, X. Qi, Y. Wang, X. Wang, S. Han, X. Liu, J. S. DuChene, H. Zhang, Q. Zhang, X. Chen, J. Ma, S. C. J. Loo, W. D. Wei, Y. Yang, J. T. Hupp and F. Huo, *Nat. Chem.*, 2012, **4**, 310–316.
- 151 Y.-H. Shih, C.-H. Chien, B. Singco, C.-L. Hsu, C.-H. Lin and H.-Y. Huang, *Chem. Commun.*, 2013, **49**, 4929–4931.
- 152 X. Yang, Z. Lin, X. Yan and Z. Cai, *RSC Adv.*, 2016, **6**, 23790–23793.
- 153 H.-L. Liu, Y.-J. Chang, T. Fan and Z.-Y. Gu, *Chem. Commun.*, 2016, **52**, 12984–12987.
- 154 L. Chen, J. Ou, H. Wang, Z. Liu, M. Ye and H. Zou, *ACS Appl. Mater. Interfaces*, 2016, **8**, 20292–20300.
- 155 Y.-H. Shih, C.-P. Fu, W.-L. Liu, C.-H. Lin, H.-Y. Huang and S. Ma, *Small*, 2016, **12**, 2057–2066.
- 156 D. Feng and Y. Xia, *Anal. Chim. Acta*, 2018, **1014**, 58–63.
- 157 Y. Zhang, Y. Song, J. Wu, R. Li, D. Hu, Z. Lin and Z. Cai, *Chem. Commun.*, 2019, **55**, 3745–3748.
- 158 K. Hu, Y. Lv, F. Ye, T. Chen and S. Zhao, *Anal. Chem.*, 2019, **91**, 6353–6362.
- 159 Z. Lin, J. Zheng, G. Lin, Z. Tang, X. Yang and Z. Cai, *Anal. Chem.*, 2015, **87**, 8005–8012.
- 160 J. Wang, J. Sun, J. Wang, H. Liu, J. Xue and Z. Nie, *Chem. Commun.*, 2017, **53**, 8114–8117.
- 161 J. Xue, H. Liu, S. Chen, C. Xiong, L. Zhan, J. Sun and Z. Nie, *Sci. Adv.*, 2018, **4**, eaat9039.
- 162 Y.-K. Kim, L.-S. Wang, R. Landis, C. S. Kim, R. W. Vachet and V. M. Rotello, *Nanoscale*, 2017, **9**, 10854–10860.
- 163 S. Huang, G. Chen, R. Ou, S. Qin, F. Wang, F. Zhu and G. Ouyang, *Anal. Chem.*, 2018, **90**, 8607–8615.
- 164 Z.-J. Zhu, P. S. Ghosh, O. R. Miranda, R. W. Vachet and V. M. Rotello, *J. Am. Chem. Soc.*, 2008, **130**, 14139–14143.
- 165 Z.-J. Zhu, R. Tang, Y.-C. Yeh, O. R. Miranda, V. M. Rotello and R. W. Vachet, *Anal. Chem.*, 2012, **84**, 4321–4326.
- 166 S. G. Elci, G. Yesilbag Tonga, B. Yan, S. T. Kim, C. S. Kim, Y. Jjiang, K. Saha, D. F. Moyano, A. L. M. Marsico, V. M. Rotello and R. W. Vachet, *ACS Nano*, 2017, **11**, 7424–7430.
- 167 S. Hou, K. N. Sikora, R. Tang, Y. Liu, Y.-W. Lee, S. T. Kim, Z. Jiang, R. W. Vachet and V. M. Rotello, *ACS Nano*, 2016, **10**, 6731–6736.

- 168 B. Yan, G. Yesilbag Tonga, S. Hou, P. W. Fedick, Y.-C. Yeh, F. S. Alfonso, T. Mizuhara, R. W. Vachet and V. M. Rotello, *Anal. Chem.*, 2014, **86**, 6710–6714.
- 169 Z.-J. Zhu, H. Wang, B. Yan, H. Zheng, Y. Jiang, O. R. Miranda, V. M. Rotello, B. Xing and R. W. Vachet, *Environ. Sci. Technol.*, 2012, **46**, 12391–12398.
- 170 F. Qiu, D. Jiang, Y. Ding, J. Zhu and L. L. Huang, *Angew. Chem., Int. Ed.*, 2008, **47**, 5009–5012.
- 171 Y. Wang, R. Du, L. Qiao and B. Liu, *Chem. Commun.*, 2018, **54**, 9659–9662.
- 172 Y. Wang, K. Zhang, X. Huang, L. Qiao and B. Liu, *Anal. Chem.*, 2021, **93**, 709–714.
- 173 X. Zhong, L. Qiao, N. Gasilova, B. Liu and H. H. Girault, *Anal. Chem.*, 2016, **88**, 6184–6189.
- 174 R. Du, L. Zhu, J. Gan, Y. Wang, L. Qiao and B. Liu, *Anal. Chem.*, 2016, **88**, 6767–6772.
- 175 W. Ma, S. Xu, H. Nie, B. Hu, Y. Bai and H. Liu, *Chem. Sci.*, 2019, **10**, 2320–2325.
- 176 H. Xu, X. Huang, Z. Zhang, X. Zhang, Q. Min and J.-J. Zhu, *Chem. Sci.*, 2020, **11**, 5280–5288.
- 177 S. Xu, W. Ma, Y. Bai and H. Liu, *J. Am. Chem. Soc.*, 2019, **141**, 72–75.
- 178 S. Xu, M. Liu, Y. Bai and H. Liu, *Angew. Chem., Int. Ed.*, 2021, **60**, 1806–1812.
- 179 Z. Baird, V. Pirro, S. Ayrton, A. Hollerbach, C. Hanau, K. Marfurt, M. Foltz, R. G. Cooks and M. Pugia, *Anal. Chem.*, 2016, **88**, 6971–6975.
- 180 X. Zhou, P. Cao, Y. Tian and J. Zhu, *J. Am. Chem. Soc.*, 2010, **132**, 4161–4168.
- 181 Z. He, Q. Chen, F. Chen, J. Zhang, H. Li and J.-M. Lin, *Chem. Sci.*, 2016, **7**, 5448–5452.
- 182 Z. Wu, L. Lin, M. Khan, W. Zhang, S. Mao, Y. Zheng, Z. Li and J.-M. Lin, *Chem. Commun.*, 2018, **54**, 11546–11549.
- 183 R. Ahmad, H. Jang, B. S. Batule and H. G. Park, *Anal. Chem.*, 2017, **89**, 8966–8973.
- 184 X.-C. Lin, X.-N. Wang, L. Liu, Q. Wen, R.-Q. Yu and J.-H. Jiang, *Anal. Chem.*, 2016, **88**, 9881–9884.
- 185 Y.-C. Liu, C.-K. Chiang, H.-T. Chang, Y.-F. Lee and C.-C. Huang, *Adv. Funct. Mater.*, 2011, **21**, 4448–4455.
- 186 Y.-J. Li, Y.-T. Tseng, B. Unnikrishnan and C.-C. Huang, *ACS Appl. Mater. Interfaces*, 2013, **5**, 9161–9166.
- 187 C.-I. Weng, J.-S. Cang, J.-Y. Chang, T.-M. Hsiung, B. Unnikrishnan, Y.-L. Hung, Y.-T. Tseng, Y.-J. Li, Y.-W. Shen and C.-C. Huang, *Anal. Chem.*, 2014, **86**, 3167–3173.
- 188 H.-W. Chu, C.-S. Lai, J.-Y. Ko, S. G. Harroun, C.-I. Chuang, R. Y. L. Wang, B. Unnikrishnan and C.-C. Huang, *ACS Sens.*, 2019, **4**, 1543–1551.
- 189 W.-J. Chiu, T.-K. Ling, H.-P. Chiang, H.-J. Lin and C.-C. Huang, *ACS Appl. Mater. Interfaces*, 2015, **7**, 8622–8630.
- 190 Y.-C. Liu, H.-T. Chang, C.-K. Chiang and C.-C. Huang, *ACS Appl. Mater. Interfaces*, 2012, **4**, 5241–5248.
- 191 Y.-J. Li, W.-J. Chiu, B. Unnikrishnan and C.-C. Huang, *ACS Appl. Mater. Interfaces*, 2014, **6**, 15253–15261.
- 192 W.-C. Chiu and C.-C. Huang, *Anal. Chem.*, 2013, **85**, 6922–6929.
- 193 Y. Zhang, B. Chen, M. He, B. Yang, J. Zhang and B. Hu, *Anal. Chem.*, 2014, **86**, 8082–8089.
- 194 X. Liu, Z.-H. Cheng, S.-Q. Zhang, N. Wu, T. Yang, M.-L. Chen and J.-H. Wang, *Anal. Chem.*, 2020, **92**, 3769–3774.
- 195 Y. He, S. Chen, L. Huang, Z. Wang, Y. Wu and F. Fu, *Anal. Chem.*, 2019, **91**, 1171–1177.
- 196 X. Zhang, R. Liu, Q. Yuan, F. Gao, J. Li, Y. Zhang, Y. Zhao, Z. Chai, L. Gao and X. Gao, *ACS Nano*, 2018, **12**, 11139–11151.
- 197 X. Zhang, R. Liu, Q. Shu, Q. Yuan, G. Xing and X. Gao, *Small*, 2018, **14**, 1703684.
- 198 S. H. Crayton, D. R. Elias, A. Al Zaki, Z. Cheng and A. Tsourkas, *Biomaterials*, 2012, **33**, 1509–1519.
- 199 C. Vancaeyzeele, O. Ornatsky, V. Baranov, L. Shen, A. Abdelrahman and M. A. Winnik, *J. Am. Chem. Soc.*, 2007, **129**, 13653–13660.